A new analytical framework for assessing the effect of sea-level rise and dredging on tidal damping in estuaries

Huayang Cai,[1] Hubert H. G. Savenije,[1] and Marco Toffolon[2]

Received 22 February 2012; revised 30 July 2012; accepted 14 August 2012; published 20 September 2012.

[1] This paper explores different analytical solutions of the tidal hydraulic equations in convergent estuaries. Linear and quasi-nonlinear models are compared for given geometry, friction, and tidal amplitude at the seaward boundary, proposing a common theoretical framework and showing that the main difference between the examined models lies in the treatment of the friction term. A general solution procedure is proposed for the set of governing analytical equations expressed in dimensionless form, and a new analytical expression for the tidal damping is derived as a weighted average of two solutions, characterized by the usual linearized formulation and the quasi-nonlinear Lagrangean treatment of the friction term. The different analytical solutions are tested against fully nonlinear numerical results for a wide range of parameters, and compared with observations in the Scheldt estuary. Overall, the new method compares best with the numerical solution and field data. The new accurate relationship for the tidal damping is then exploited for a classification of estuaries based on the distance of the tidally averaged depth from the ideal depth (relative to vanishing amplification) and the critical depth (condition for maximum amplification). Finally, the new model is used to investigate the effect of depth variations on the tidal dynamics in 23 real estuaries, highlighting the usefulness of the analytical method to assess the influence of human interventions (e.g. by dredging) and global sea-level rise on the estuarine environment.

Citation: Cai, H., H. H. G. Savenije, and M. Toffolon (2012), A new analytical framework for assessing the effect of sea-level rise and dredging on tidal damping in estuaries, *J. Geophys. Res.*, *117*, C09023, doi:10.1029/2012JC008000.

1. Introduction

[2] Tidal dynamics in estuaries have long been the subject of intensive scientific interest and have received increasing attention to analyze the environmental impact of human interventions. In many estuaries, there are increasing concerns about the impacts on the estuarine environment of, e.g., sea-level rise, water diversion and dredging. However, before predictions about hydraulic responses to future changes can be made with any confidence, there is a need to achieve an adequate understanding of tidal wave propagation in estuaries.

[3] Due to the advances in computational hydraulics, tidal wave propagation in estuaries can be accurately simulated by numerical models. However, unlike analytical models, numerical models do not provide direct insight into the effect that controlling parameters (e.g., geometry and forcing) have on tidal variables, such as flow velocity, water level, wave celerity, phase lag or tidal damping. Ever since *Lorentz* [1926] linearized the bottom friction term, simple solutions have been found to describe tidal dynamics with the linearized one-dimensional St. Venant equations. Several analytical solutions for convergent channels were developed, using different forms of linearization [e.g., *Jay*, 1991; *Friedrichs and Aubrey*, 1994; *Lanzoni and Seminara*, 1998; *Savenije*, 1998; *Prandle*, 2003, 2009; *Savenije et al.*, 2008; *Friedrichs*, 2010; *Toffolon and Savenije*, 2011; *Van Rijn*, 2011]. Most researchers linearized the hydrodynamic equations by means of a perturbation analysis or by linearizing the friction term. Conversely, *Savenije* [1998] derived expressions for the envelope curves of high water (HW) and low water (LW) to arrive at a damping equation that retained the quadratic dependence of friction on velocity as well as the effect of the periodic variation of the hydraulic radius, still assuming that the tidal amplitude to depth ratio is small and that the tidal velocity can be described by a simple harmonic with variable amplitude (hence we will term this as quasi-nonlinear model). On the basis of this quasi-nonlinear model, *Savenije et al.* [2008] provided a fully explicit solution of the tidal hydraulic equations.

[4] Recently, *Toffolon and Savenije* [2011] proposed a modified linear model and compared it with the quasi-nonlinear model of *Savenije et al.* [2008], suggesting that the discontinuous behavior (i.e., with two families of solutions)

[1]Department of Water Management, Delft University of Technology, Delft, Netherlands.
[2]Department of Civil and Environmental Engineering, University of Trento, Trento, Italy.

Corresponding author: H. Cai, Department of Water Management, Faculty of Civil Engineering and Geosciences, Delft University of Technology, Stevinweg 1, PO Box 5048, 2600 GA Delft, Netherlands. (h.cai@tudelft.nl)

0148-0227/12/2012JC008000

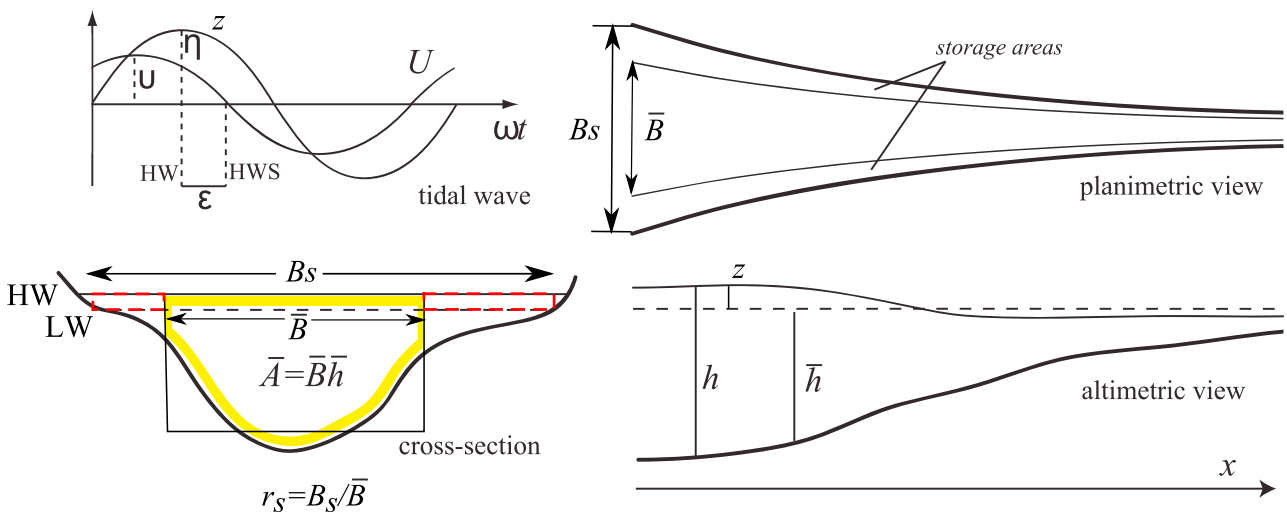

Figure 1. Sketch of the geometry of the idealized tidal channel and notation: tidal oscillations of water level z and velocity U and definition of the phase lag ϵ; definition of the equivalent rectangular cross-section of width B, and of the total width B_s including storage areas; planimetric view of the estuary with storage areas; lateral view showing instantaneous and tidally averaged depth. Modified from *Savenije et al.* [2008].

and the transition toward a standing wave (i.e., the wave celerity tending toward infinity) predicted by the latter model do not happen in reality. Interestingly, numerical simulations (see section 3.2) indicate that the two models approach the numerical results from a different side, i.e., the modified linear model overestimates the tidal damping while the quasi-nonlinear model underestimates it, and it appears that a weighted average of the two comes close to the numerical results. In the present contribution, a comparison is made between different linear and quasi-nonlinear models building a common theoretical framework based on which a new analytical model is derived. We pay particular attention to the effect of different formulations of the friction term, leading to different expressions for tidal damping.

[5] Of course, analytical approaches to describe a real complex estuarine system comprise several limitations, like for instance the highly simplified geometry of the cross-section, the idealized planimetric shape, the assumption of small tidal amplitude, the neglect of Coriolis force and density gradients. Nevertheless, the advantages are many. First of all, the analytical equations provide direct insight into the effect of model forcing and geometry on system performance (e.g., to assess the effects of dredging on tidal dynamics). Second, they form a simple and rapid assessment tool in the preparation of a more complex numerical modeling exercise (e.g., to assess the possible outcome of a numerical model or to design the model setup). Finally, they can be very useful in setting up a monitoring program and to identify the most effective density and location of the monitoring network.

[6] The paper is arranged as follows. In the next section, we present the basic equations of tidal wave propagation in convergent estuaries. The comparison between the quasi-nonlinear model and the linear model is presented in section 3. In section 4, the performance of the new analytical model is shown and compared with analytical solutions by *Savenije et al.* [2008], *Toffolon and Savenije* [2011] and Dronkers' approach [*Dronkers*, 1964]. The new model is subsequently applied in the Scheldt estuary and compared with the solution of a numerical model. In section 5, a new classification of estuaries and the effect of depth variations on tidal dynamics in 23 real estuaries are presented. Finally, conclusions are drawn in section 6.

2. Basic Equations of Estuarine Tidal Dynamics

[7] We consider a tidal channel with varying width and depth and investigate the propagation of the tidal wave along an estuary with a fixed bed. The conceptual sketch of the geometry of the idealized tidal channel is presented in Figure 1, together with a simplified picture of the periodic oscillations of water level and velocity defining the phase lag. In order to derive a simple analytical solution, we assume that the flow is concentrated in a main rectangular cross-section, with possible presence of lateral storage areas, described by the storage width ratio $r_s = B_s/\overline{B}$, i.e., the ratio between the storage width B_s and the stream width $\overline{B}$ (see Figure 1).

[8] In alluvial estuaries, the tidally averaged cross-sectional area $\overline{A}$ can be described by an exponential function [*Savenije*, 1992a]:

$$\overline{A} = \overline{A_0}\exp\left(-\frac{x}{a}\right), \tag{1}$$

where a is the convergence length, $\overline{A_0}$ is the cross-sectional area at the estuary mouth and x is the longitudinal coordinate measured in landward direction from the estuary mouth. In several practical cases, it is reasonable to assume that the depth convergence is small compared with the width convergence, and hence the convergence length a is approximately equal to the width convergence length.

[9] The basic one-dimensional equations describing the tidal dynamics in an estuary are the continuity and momentum equations [e.g., *Savenije*, 2005], which read:

$$\frac{\partial U}{\partial t} + U\frac{\partial U}{\partial x} + g\frac{\partial h}{\partial x} + gI_b + gF + \frac{gh}{2\rho}\frac{\partial \rho}{\partial x} = 0, \tag{2}$$

$$r_s\frac{\partial z}{\partial t} + U\frac{\partial z}{\partial x} + h\frac{\partial U}{\partial x} - \frac{hU}{a} = 0, \tag{3}$$

where t is the time, U is the cross-sectional average flow velocity, h is the flow depth, g is the acceleration due to gravity, I_b is the bottom slope, ρ is the water density, z is the free surface elevation, and F is the friction term. The friction term is widely represented by:

$$F = \frac{U|U|}{K^2 h^{4/3}}, \tag{4}$$

where K is the Manning-Strickler friction coefficient. The density gradient described by the last term in the left-hand side of equation (2) is often disregarded, but in the method of *Savenije et al.* [2008] it is retained (see also Appendix A).

[10] The system is forced by a sinusoidal tidal wave with a tidal period T and a frequency $\omega = 2\pi / T$. As the wave propagates into the estuary, it has a wave celerity c, an amplitude of the tidal water level variation η, a tidal velocity amplitude υ, and a phase lag ϵ, defined as the phase difference between high water (HW) and high water slack (HWS), or between low water (LW) and low water slack (LWS) due to the assumption of a simple harmonic solution(see Figure 1). After scaling the continuity and momentum equations (2) and (3), five dimensionless variables can be found: the estuary shape number γ (representing the effect of depth and width convergence), the friction number χ (describing the role of the frictional dissipation), the velocity number μ (the actual velocity scaled with the frictionless value in a prismatic channel), the celerity number λ (the ratio between the theoretical frictionless celerity in a prismatic channel and the actual wave celerity), and the damping number for tidal amplitude δ (a dimensionless description of the increase, $\delta > 0$, or decrease, $\delta < 0$, of the tidal wave amplitude along the estuary) [*Toffolon et al.*, 2006; *Savenije et al.*, 2008], where γ and χ are the independent variables, while ϵ, μ, λ, δ are the dependent variables. For further details on the scaling factors and the resulting dimensionless equations, readers can refer to *Savenije et al.* [2008]. These dimensionless variables are defined as:

$$\gamma = \frac{c_0}{\omega a}, \tag{5}$$

$$\chi = r_s f \frac{c_0}{\omega \bar{h}}\zeta, \tag{6}$$

$$\mu = \frac{1}{r_s}\frac{\upsilon \bar{h}}{\eta c_0}, \tag{7}$$

$$\lambda = \frac{c_0}{c}, \tag{8}$$

$$\delta = \frac{1}{\eta}\frac{d\eta}{dx}\frac{c_0}{\omega}, \tag{9}$$

where c_0 is the classical wave celerity of a frictionless progressive wave, $\bar{h}$ is the tidal average depth of flow, f is the dimensionless friction factor and ζ is the dimensionless tidal amplitude defined as:

$$c_0 = \sqrt{g\bar{h}/r_s}, \tag{10}$$

$$f = \frac{g}{K^2 \bar{h}^{1/3}}\left[1 - \left(\frac{4}{3}\zeta\right)^2\right]^{-1}, \tag{11}$$

$$\zeta = \frac{\eta}{\bar{h}}. \tag{12}$$

[11] In equation (11), the periodic effect of depth variation during the tidal cycle has been taken into account through the factor indicated between square brackets, which results from the subtraction of the envelopes at HW and LW. This additional friction factor is a property of the envelope method [e.g., *Savenije*, 2005], which traditional linearization methods do not have. For small value of tidal amplitude to depth ratio ($\zeta \ll 1$), this property is less important. Making use of these dimensionless parameters, *Savenije et al.* [2008] derived four dimensionless equations based on the equations for the phase lag [*Savenije*, 1992a, 1993], for tidal damping [*Savenije*, 1998, 2001], and for wave propagation [*Savenije and Veling*, 2005]:

$$\delta = \frac{\gamma}{2} - \frac{1}{2}\chi\mu^2, \tag{13}$$

$$\mu = \frac{\sin(\epsilon)}{\lambda} = \frac{\cos(\epsilon)}{\gamma - \delta}, \tag{14}$$

$$\tan(\epsilon) = \frac{\lambda}{\gamma - \delta}, \tag{15}$$

$$\lambda^2 = 1 - \delta(\gamma - \delta). \tag{16}$$

[12] The damping equation (13) reflects the relative balance between the convergence of banks and friction and can be rewritten as:

$$\gamma - \delta = \frac{\gamma + \chi\mu^2}{2}, \tag{17}$$

which is greater than 0 for any convergent estuary ($\gamma > 0$), showing that the tidal wave amplification (δ) cannot be larger than the estuary shape number γ. The scaling equation (14) shows that the velocity amplitude is determined by the ratio between the phase lag ϵ and the combined effect of friction and convergence as expressed in (17). The phase lag equation (15) highlights that a standing wave ($\epsilon = 0$) is characterized by an infinite wave celerity ($\lambda \to 0$) and that friction tends to move the system far from this asymptotic condition. On the other hand, a progressive wave ($\epsilon = \pi / 2$)

Table 1. Comparison of Different Approaches to Tidal Damping Equation

Model	Method	Landward b.c.	$U\partial U / \partial x$ and $gh / (2\rho)\partial\rho / \partial x$	Friction Term	Damping Equation
Savenije et al. [2008]	Subtracting high water and low water envelopes	Neglected	Considered	Quadratic velocity, time-variable depth	$\delta = \frac{\gamma}{2} - \frac{1}{2}\chi\mu^2$
Toffolon and Savenije [2011], *Van Rijn* [2011]	Considering the amplitude of complex function	Neglected (but possibly considered)	Neglected	Linearized, time-invariant depth	$\delta = \frac{\gamma}{2} - \frac{1}{\sqrt{2}}\sqrt{\Gamma + \sqrt{\Gamma^2 + \left(\frac{8}{3\pi}\chi\mu\right)^2}}$ $\Gamma = \frac{\gamma^2}{4} - 1$ (T1)
Van Rijn [2011]	Energy-based approach	Neglected	Neglected	Linearized, time-invariant depth	$\delta = \frac{\gamma}{2} - \frac{4}{3\pi}\frac{\chi\mu}{\lambda}$ (T2)

is obtained only when the difference between γ and δ (17) is vanishingly small, i.e., when both friction and convergence are negligible. The celerity equation (16) shows that tidal wave propagation is closely related with the longitudinal amplitude variation (amplification or damping): recalling the positive value of (17), it is easy to see that the actual celerity c is larger than the reference value c_0 for amplified conditions, while it decreases with damping. It is worth noting that this set of equations corresponds to the case of an infinitely long channel, where the effect of the landward boundary condition can be neglected [*Toffolon and Savenije*, 2011]. Also it is worth noting that in the derivation of both the damping and the celerity equation, the density term in the momentum balance equation was taken into account, but that this term dropped out in both the envelope method [*Savenije*, 1998, 2001] and the method of characteristics [*Savenije and Veling*, 2005] used for their derivation. Hence the density term has no impact on the tidal damping nor the wave celerity. The scaling equation and the phase lag equation result from the mass balance equation and hence are also not affected by the density term.

3. Comparison Between Linear and Quasi-nonlinear Solutions

3.1. Difference in Damping Equation

[13] Recently, *Toffolon and Savenije* [2011] and *Van Rijn* [2011] revisited the linear solution for estuarine hydrodynamics by taking into account the effects of the width and depth convergence. In this section we compare these modified linear solutions with the quasi-nonlinear analytical solution proposed by *Savenije et al.* [2008], with specific focus on the damping equation (Table 1). Basically, *Toffolon and Savenije* [2011] and *Van Rijn* [2011] exploited the same method, linearizing the friction term (both the velocity variation $U|U|$ and the variation of the depth h) and neglecting the inertial term $U\partial U / \partial x$ and the density term $gh / (2\rho)\partial\rho / \partial x$ in the momentum balance equation. The set of obtained equations was then solved using complex functions. These functions were considered as a local approximation of the solution in a multi-reach system by *Toffolon and Savenije* [2011], who also showed a more reliable solution can be obtained by iteratively refining the Lorentz constant in the friction term. On the other hand, *Van Rijn* [2011] concentrated on the solution of the whole estuary, but derived a damping equation based on energy considerations as well. Another distinct difference is that the solution proposed by *Savenije et al.* [2008] is intrinsically local, i.e., it is expressed in terms of point-to-point values of the parameters provided that the information about the tidal amplitude is transferred only in the landward direction by means of the damping equation, while the other two linearized solutions (which potentially account also for the landward boundary condition) can be used in this way by neglecting the effect of the reflected wave.

[14] It is worth noting that, after some algebra, it is possible to demonstrate that the two damping equations (T1, T2) in Table 1 are identical, which means that the analytical solution proposed by *Van Rijn* [2011], both with the linear and the energy-based approach, can be cast into the same set of four nonlinear equations using the dimensionless parameters defined in section 2. The dimensionless equations

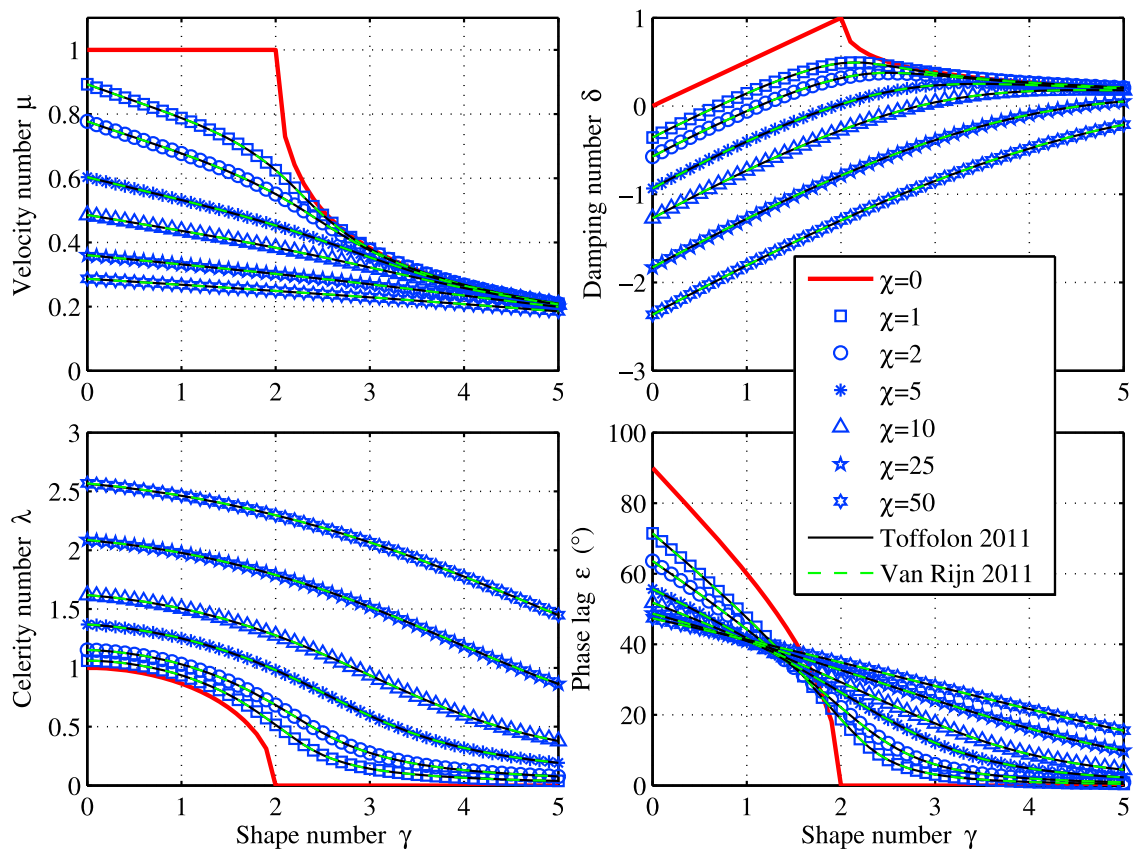

Figure 2. Relationship between the main dimensionless parameters and the estuary shape number γ (5) obtained by solving equation (18) in combination with equations (15), (14), and (16) for different values of the friction number χ (6). The drawn black and dashed green lines represent the solutions obtained by *Toffolon and Savenije* [2011] and *Van Rijn* [2011], respectively.

obtained are similar to equations (13)–(16), but with a different damping equation:

$$\delta = \frac{\gamma}{2} - \frac{4}{3\pi}\frac{\chi\mu}{\lambda}. \tag{18}$$

Since *Van Rijn*'s [2011] model is characterized by Lorentz's linearization [*Lorentz*, 1926] of the friction term F:

$$F_L = \frac{8}{3\pi}\frac{v}{K^2\overline{h}^{4/3}}U, \tag{19}$$

it is interesting to analyze the effect of using Lorentz's assumption in the derivation of the damping equation (13) with the envelope method. This is done in Appendix A, following the procedure proposed by *Savenije* [2005] and considering the linearized friction term, instead of the quasi-nonlinear friction term, in the momentum equation. The result is that we obtain the same linear tidal damping equation as in (18), demonstrating that *Van Rijn*'s [2011] model coincides with the linearized version of *Savenije et al.* [2008].

[15] Replacing the quasi-nonlinear damping equation (13) with equation (18), a new system of four analytical equations is obtained, namely (18), (14), (15) and (16). In contrast to the quasi-nonlinear system, which has an explicit solution, this set of equations can only be solved by an iterative numerical method (e.g., a simple Newton-Raphson method). Figure 2 shows the variation of the dependent dimensionless parameters obtained with the different approaches as a function of the estuary shape number γ and the friction number χ. We can see that the results obtained using (18) coincide fully with the solutions provided by *Van Rijn* [2011] and *Toffolon and Savenije* [2011]. Hence, the only difference between the quasi-nonlinear [*Savenije et al.*, 2008] and modified linear models [*Toffolon and Savenije*, 2011; *Van Rijn*, 2011] is the friction term in the damping equation.

[16] More precisely, the damping equation of *Savenije et al.* [2008] differs from the linearized damping equation by a factor that depends on the phase lag ϵ, as becomes clear by substituting (14) into (13):

$$\delta = \frac{\gamma}{2} - \frac{1}{2}\frac{\chi\mu}{\lambda}\sin(\epsilon) \tag{20}$$

Equations (18) and (20) are formally identical if $\sin(\epsilon) = 8/(3\pi) \approx 0.85$, implying a value of the phase lag of approximately 58° (2 hours for an M2 tide).

[17] *Dronkers* [1964, p. 302] suggested an interesting higher order formulation for the friction term [see also *Cartwright*, 1968], leading to results that are comparable to those obtained using the fully nonlinear formulation for the friction term. *Dronkers* [1964] took account of over-tide

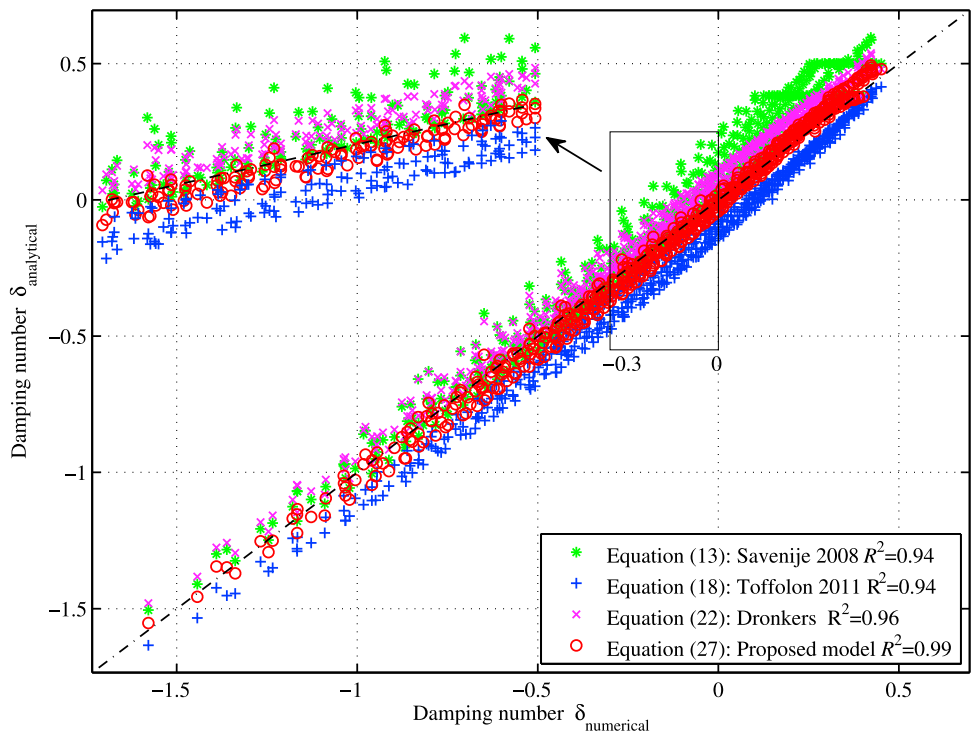

Figure 3. Tidal damping δ at $x^* = 0.426$ obtained with four different analytical models (new damping equation (27), Dronkers' equation (22), *Savenije et al.* [2008], *Toffolon and Savenije* [2011]), compared to numerical results. R^2 is the coefficient of determination, which provides an estimate of the average deviation of the estimates of the different analytical models from the assumed correct value (numerical model): the closer R^2 is to unit, the better is the model.

generation by including a third order term (cubic velocity) in the friction term, while also assuming that U is a periodic function with zero mean:

$$F_D = \frac{16}{15\pi}\frac{\upsilon^2}{K^2\overline{h}^{4/3}}\left[\frac{U}{\upsilon} + 2\left(\frac{U}{\upsilon}\right)^3\right]. \tag{21}$$

Note that this equation did not account for the time variable depth in the friction term. In our symbols the expression for the tidal damping using Dronkers' friction term would read (see Appendix B):

$$\delta = \frac{\gamma}{2} - \frac{8}{15\pi}\frac{\chi\mu}{\lambda} - \frac{16}{15\pi}\chi\mu^3\lambda. \tag{22}$$

Equation (22), when combined with equations (14), (15) and (16), forms a new set of nonlinear equations, which can be solved iteratively.

[18] It is worth noting that the different methods use different definitions of the dimensionless friction factor f (i.e., equation (11)). The Lorentz's linearization and Dronkers' method consider a time-invariant depth in the friction term, which is the same as taking $\zeta = 0$ in (11), i.e., $f = g/(K^2\overline{h}^{1/3})$.

3.2. Performance of Different Analytical Models

[19] In order to investigate the performance of the analytical solutions, they have been compared with a fully nonlinear numerical solution of the governing equations (2) and (3). The numerical model [*Toffolon et al.*, 2006] is based on the explicit MacCormack method, which is second order accurate both in space and in time. A total variation diminishing (TVD) filter is applied to avoid spurious oscillations, especially when the wave steepens because of frictional or geometrical effects.

[20] Since we focus on the tidal damping in this paper, in this section we present a comparison between the values of the dimensionless damping number δ estimated using analytical methods against the fully nonlinear numerical results. We consider a wide range of parameters (with $1 \le \gamma \le 3$, $0.1 \le \zeta \le 0.3$, $10\ \mathrm{m}^{1/3}\ \mathrm{s}^{-1} \le K \le 50\ \mathrm{m}^{1/3}\ \mathrm{s}^{-1}$ and $\overline{h} = 10$ m) covering a wide spectrum of tidal channels. In order to present dimensionless results, distance x is scaled by the frictionless wavelength in prismatic channels:

$$x^* = \frac{\omega}{c_0}x \tag{23}$$

[21] Figure 3 shows the performance of the different analytical models at a single position $x^* = 0.426$ (corresponding to 30 km for a 10 m deep estuary). Both the linear [*Toffolon and Savenije*, 2011] and the quasi-nonlinear [*Savenije et al.*, 2008] solution behave reasonably well, but none of them is fully correct for a finite amplitude wave. It appears that Dronkers' approach lies closest to the numerical solution, and that *Savenije et al.* [2008] and *Toffolon and Savenije* [2011] have a consistent bias from the numerical solution. The former method underestimates the tidal damping, while the latter overestimates it.

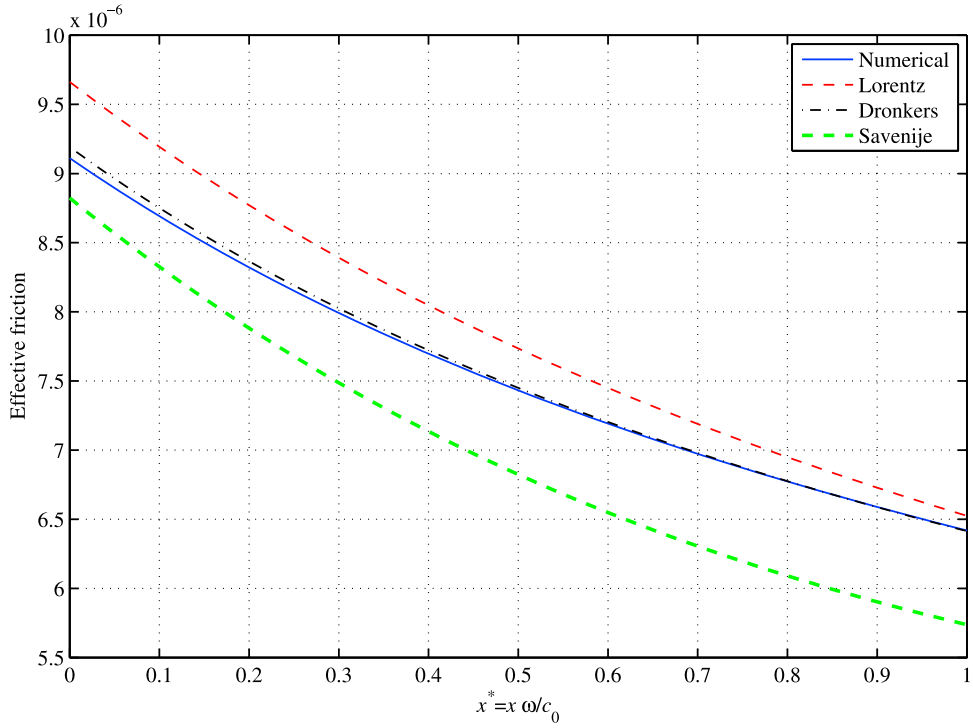

Figure 4. Comparison of the tidally averaged friction term $\langle |F| \rangle$ computed with different formulations of the friction term: fully nonlinear (4) (blue line), Lorentz's linearization (19) (red dashed line), Dronkers' expansion (21) (black dash-dot line); and for Savenije's effective friction $\hat{F}_S$ (24) (green dashed line). All estimates are based on variables obtained from numerical results (γ = 1, ζ = 0.1, K = 30 m$^{1/3}$ s^{-1} and $\overline{h}$ = 10 m).

[22] The reason for this behavior lies in the different simplifications used in the friction term *F. Toffolon and Savenije* [2011] used Lorentz's linearization (19), which is based on the equal energy dissipated by linear and quadratic friction during a tidal cycle (assuming a sinusoidal tide). On the other hand, working within an original Lagrangean-based approach, *Savenije et al.* [2008] obtained the effective friction $\hat{F}_S$ acting over a tidal cycle by subtracting the high water (HW) and low water (LW) envelopes, leading to:

$$\hat{F}_S = \frac{1}{2}\left[\frac{U_{HW}^2}{K^2\left(\overline{h}+\eta_{HW}\right)^{4/3}} + \frac{U_{LW}^2}{K^2\left(\overline{h}-\eta_{LW}\right)^{4/3}}\right], \qquad (24)$$

where the two velocities at HW and LW follow from:

$$U_{HW} \approx \upsilon \sin(\epsilon), \quad U_{LW} \approx -\upsilon \sin(\epsilon). \qquad (25)$$

[23] These approaches (linearized and quasi-nonlinear), which are correct for the strictly linear case where the tidal wave is a simple harmonic, yield opposite biases in the damping equation for finite-amplitude waves.

[24] This behavior can be clearly seen from Figure 4, which compares the friction effectively acting during a tidal cycle considering the different options. The damping in the three standard Eulerian approaches [see also *Vignoli et al.*, 2003] is based on the definition of a tidally average friction term $\langle |F| \rangle = T^{-1}\int_T |F| dt$, where F is estimated as follows: the fully nonlinear definition from (4) (blue line), Lorentz's linearization F_L from (19) (red dashed line), and Dronkers' relationship F_D from (21) (black dash-dot line). On the contrary, Savenije's Lagrangean approach (24) directly provides the effective friction $\hat{F}_S$ (green dashed line), which can be consistently compared with the previous ones. All quantities used in Figure 4 are obtained by the numerical model, so the only difference is the approximation used for the friction term. The comparison suggests that the tidally averaged friction term obtained with Lorentz's linearization overestimates the friction along the estuary, while *Savenije et al.* [2008] model tends to underestimate it. In the middle, the third-order approximation by *Dronkers* [1964] is very close to the complete nonlinear friction.

[25] As a whole, the two approaches to calculate the frictional dissipation (i.e., using the linearized friction term or the average of HW and LW values) consistently have an opposite bias. Because of this, it is attractive to explore if the 'true' damping can be obtained by taking the weighted average of equations (18) and (20):

$$\delta = \frac{\gamma}{2} - \alpha\frac{4}{3\pi}\frac{\chi\mu}{\lambda} - (1-\alpha)\frac{1}{2}\chi\mu^2. \qquad (26)$$

[26] For different weights of the linearized friction term α (from 0 to 1), it is possible to compare the values of δ obtained by equation (26) with the damping observed in the

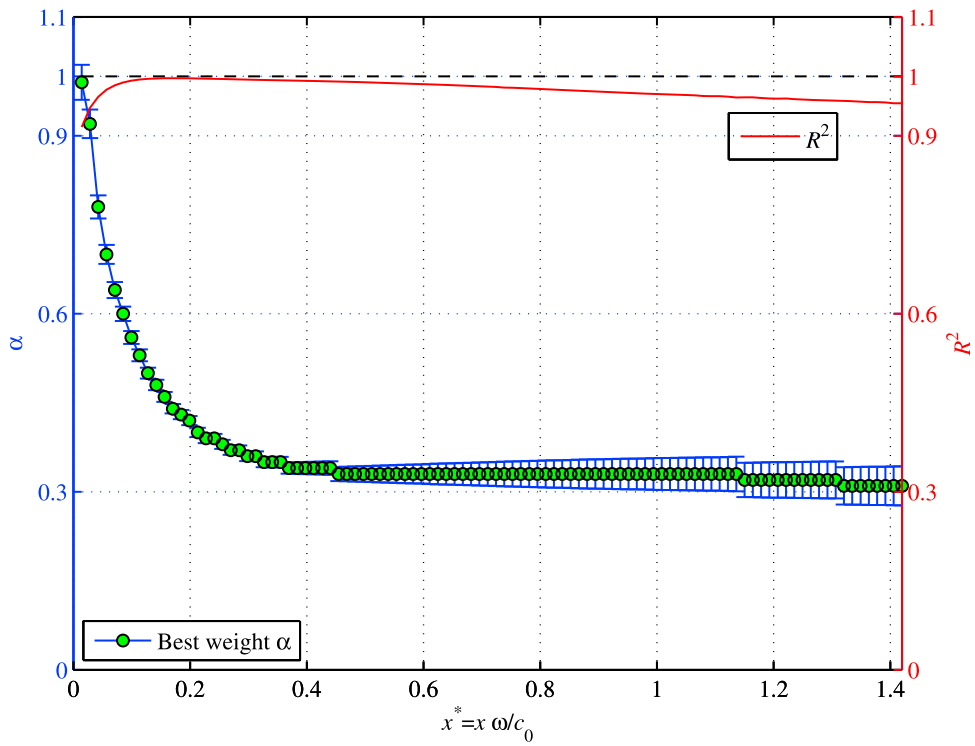

Figure 5. Optimum weight of the linearized friction term α with its standard error along the estuary axis and the corresponding coefficient of determination R^2.

numerical results for the same wide range of parameters as for Figure 3. Figure 5 presents the optimum weight α with its standard error at different locations along the estuary and the corresponding coefficient of determination R^2. We can see that the optimum weight α becomes stable from $x^* \simeq 0.35$ onward and that the equilibrium weight for α is about 1/3. The fact that the weight is approximately 1 (corresponding to the linearized friction) near the estuary mouth is the result of the imposed harmonic boundary condition without overtides, which is consistent with the linear assumption. The stable values of α that develops in the landward direction indicates that the wave adjusts its shape toward an equilibrium shape.

[27] Assuming $\alpha = 1/3$, the optimized damping equation hence reads:

$$\delta = \frac{\gamma}{2} - \frac{4}{9\pi}\frac{\chi\mu}{\lambda} - \frac{\chi\mu^2}{3}. \tag{27}$$

This equation is very similar to Dronkers' equation (22), which can be rearranged using (14) in the following form:

$$\delta = \frac{\gamma}{2} - \frac{2}{5}\frac{4}{3\pi}\frac{\chi\mu}{\lambda} - \frac{32}{15\pi}\sin(\epsilon)\frac{1}{2}\chi\mu^2. \tag{28}$$

Similarly to (26), the last two terms of equation (28) can be seen as a combination of (18) and (20), whereby the weights of the linearized and nonlinear models imply $\alpha = 0.4$ and $1 - \alpha = 0.68\ \sin(\epsilon)$, which is satisfied if $\sin(\epsilon) \simeq 0.88$, a value similar to the one derived from (20).

[28] By iteratively solving the set of four analytical equations (14), (15), (16) and (27), we have obtained a new analytical solution for the dimensionless parameters μ, δ, λ, and ϵ. The damping number δ has been compared with the other solutions in Figure 3, and we can see that the agreement of equations (22) and (27) with the numerical model is very good, but the latter obtains the best result with the highest coefficient of determination $R^2 = 0.99$. Moreover, as we can see from Figure 6, where different versions of analytical solutions are compared with numerical results, the proposed new damping equation obtains the best result with the highest coefficient of determination R^2 along the estuary axis, except near the mouth of the estuary where the modified linear model [*Toffolon and Savenije*, 2011] achieves the best result due to the purely harmonic wave imposed at the seaward boundary.

[29] Apparently, by combining the two approaches of *Toffolon and Savenije* [2011] and *Savenije et al.* [2008], we have obtained a more accurate analytical model, which is closer to the fully nonlinear numerical solution.

4. Behavior of the New Set of Equations

4.1. General Performance

[30] Figures 7–10 present the solution of the velocity number, the damping number, the celerity number, and the phase lag obtained with the different analytical models as a function of γ and χ. In these graphs, the blue symbols represent the new method using equation (27), whereas the dashed red lines represent the solution of *Savenije et al.* [2008], the drawn black lines the solution of *Toffolon and Savenije* [2011], and the dashed-dotted green lines the solution with Dronkers' friction term. Unlike the equation of *Savenije et al.* [2008], which had two families of solutions

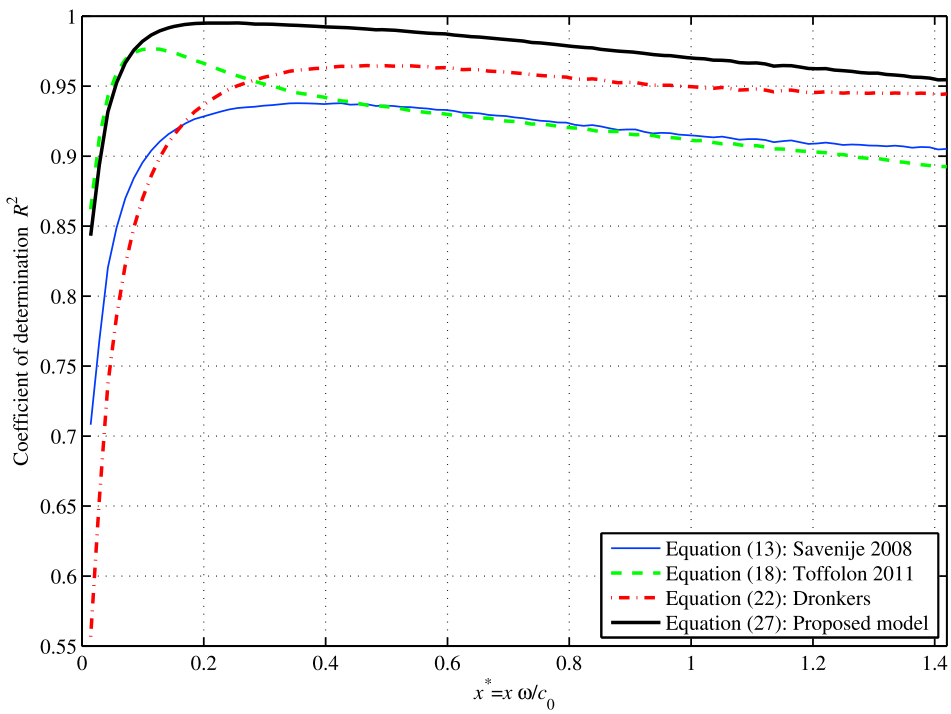

Figure 6. Longitudinal variation of the coefficient of determination R^2 between numerical model and different analytical models for a wide range of parameters with $1 \leq \gamma \leq 3$, $0.1 \leq \zeta \leq 0.3$, $10\ \mathrm{m}^{1/3}\ \mathrm{s}^{-1} \leq K \leq 50\ \mathrm{m}^{1/3}\ \mathrm{s}^{-1}$ and $\overline{h} = 10$ m.

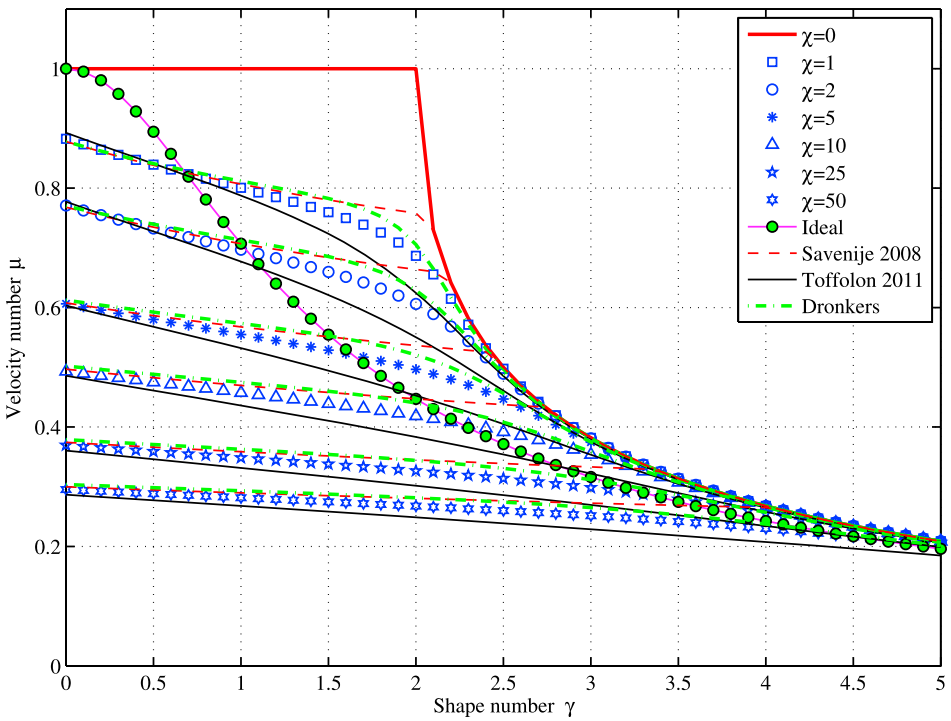

Figure 7. Relationship between the velocity number μ (7) and the estuary shape number γ (5) for different values of the friction number χ (6). The blue symbols indicate the new model exploiting equation (27). The red drawn line represents the frictionless estuary ($\chi = 0$). The dashed red lines, drawn black lines, and dashed-dotted green lines represent the solutions obtained by *Savenije et al.* [2008], *Toffolon and Savenije* [2011], and Dronkers' approach, respectively. The green round symbols indicate the ideal estuary $\left(\mu = \sqrt{\frac{1}{1+\gamma^2}}\right)$.

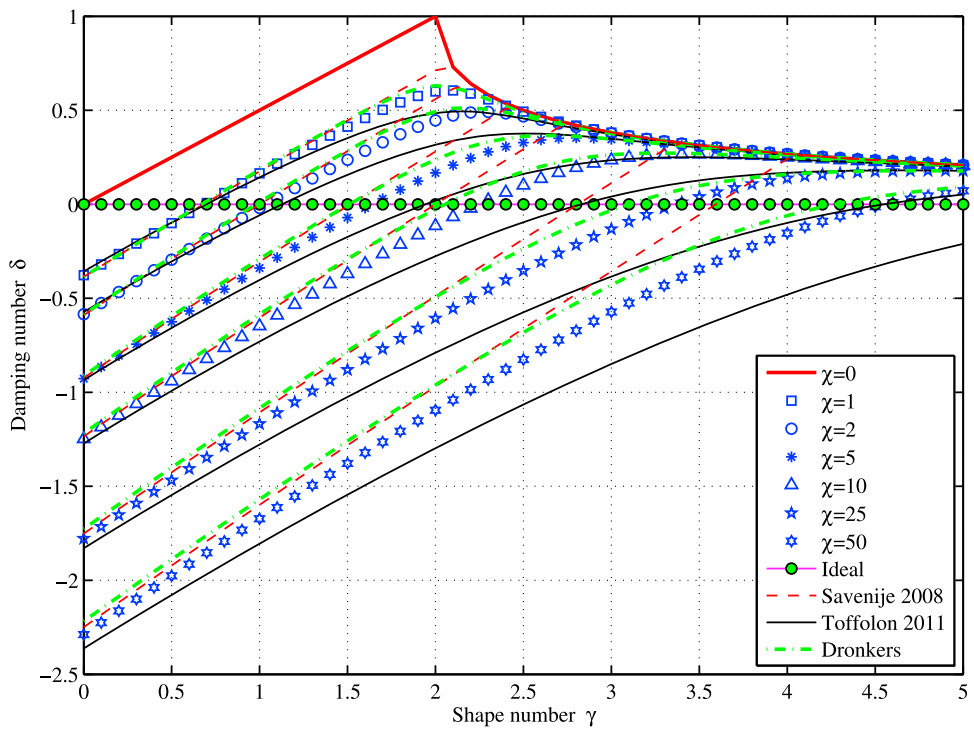

Figure 8. Relationship between the damping number δ (9) and the estuary shape number γ (5) for different values of the friction number χ (6). The symbols are as in Figure 7. The ideal estuary is defined by $\delta = 0$.

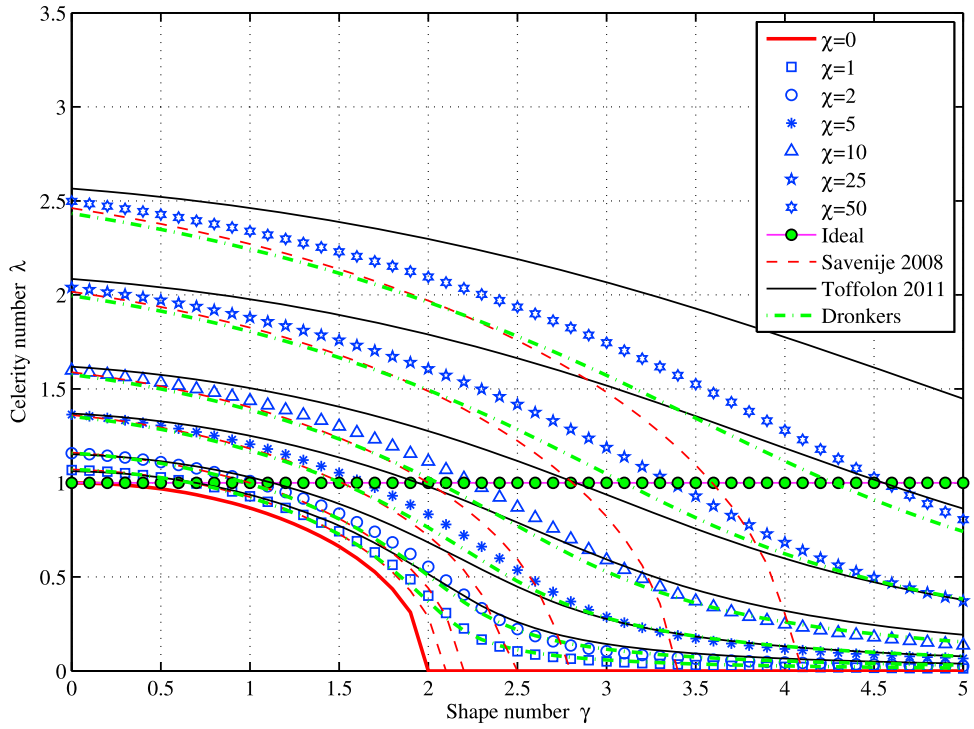

Figure 9. Relationship between the celerity number λ (8) and the estuary shape number γ (5) for different values of the friction number χ (6). The symbols are as in Figure 7. The ideal estuary is defined by $\lambda = 1$.

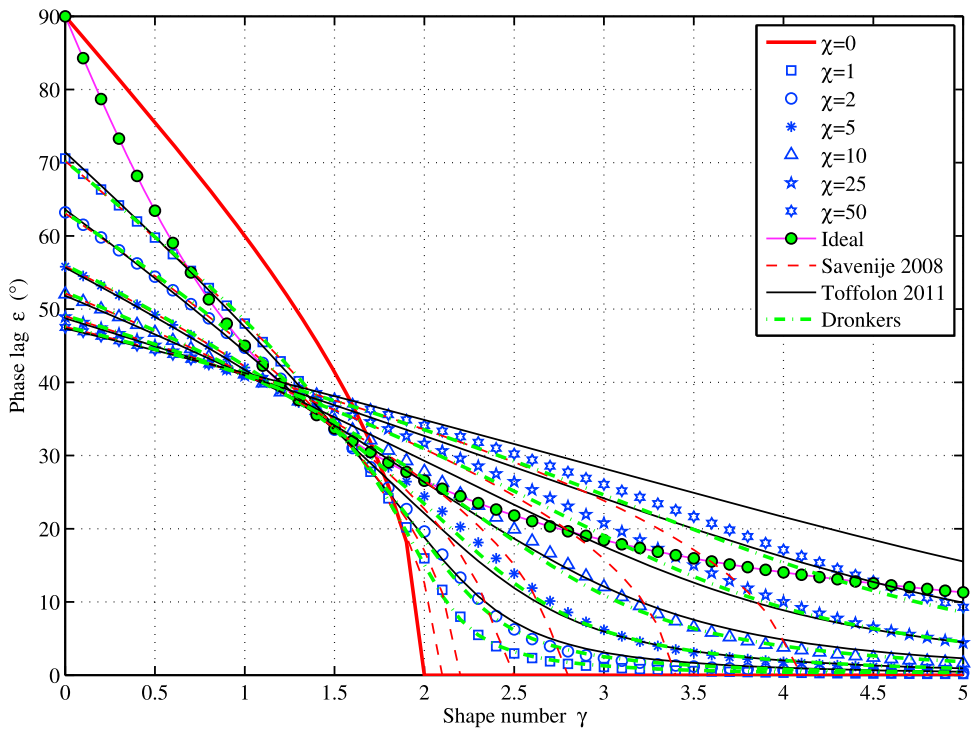

Figure 10. Relationship between the phase lag ϵ and the estuary shape number γ (5) for different values of the friction number χ (6). The symbols are as in Figure 7. The ideal estuary is defined by $\epsilon = \arctan(1/\gamma)$.

for mixed and standing waves, both the new solution and the solutions of *Toffolon and Savenije* [2011] and Dronkers' approach provide continuous solutions in the transition zone of critical convergence [*Jay*, 1991] where γ is close to 2. In the new model, a clear separation between the subcritical and the supercritical cases exists only for vanishing friction ($\chi = 0$).

[31] Comparing the new model with the other three models, we can see in Figures 7–10 that three zones can be distinguished. For small values of γ (weakly convergent estuaries), the main dimensionless parameters (μ, δ, λ and ϵ) obtained with the new model are closer to the linear solution of *Toffolon and Savenije* [2011]. In the transition zone where critical convergence occurs in the model of *Savenije et al.* [2008], the result is about the average of *Savenije et al.* [2008] and *Toffolon and Savenije* [2011]. For larger values of γ (the strongly convergent estuaries), we can see that the new solution is closer to the frictionless case. Moreover, it appears that Dronkers' solution is very close to our new solution for an amplified wave with bigger γ, while it is similar to *Savenije et al.* [2008] for waves with $\gamma < 2$. For an ideal estuary (where friction balances convergence), the four methods are identical.

4.2. Application to the Scheldt Estuary

[32] For given geometry, friction, and tidal amplitude at the downstream boundary, the dimensional values of the tidal amplitude η, the velocity amplitude υ, the wave celerity c, and the phase lag ϵ can be computed by using the analytical model presented in section 3. We have applied the new equation to the geometry of the Scheldt estuary, assuming a convergence length for the cross-sectional area a = 27 km [see also *Horrevoets et al.*, 2004]. Until 110 km from the mouth of the estuary the flow depth is approximately constant ($\bar{h}$ = 11 m), while more landward the depth reduces gradually to 2.6 m (assumed estuary length L = 200 km). At the estuary mouth (x = 0 m), we assume a harmonic tide characterized by a tidal amplitude η_0 = 2.3 m (spring tide) and a tidal period T = 44400 s.

[33] The four analytical models have been compared with observations made in the Scheldt estuary during spring tide on 14–15 June 1995. The different models can be made to fit the observations if a suitable friction coefficient is used. However, this calibration provided significantly different values of the Manning-Strickler coefficient: $K = 32\ \mathrm{m}^{1/3}\ \mathrm{s}^{-1}$ for *Savenije et al.*'s [2008] model, $K = 33\ \mathrm{m}^{1/3}\ \mathrm{s}^{-1}$ for Dronkers' approach, $K = 39\ \mathrm{m}^{1/3}\ \mathrm{s}^{-1}$ for the present model, and $K = 46\ \mathrm{m}^{1/3}\ \mathrm{s}^{-1}$ for *Toffolon and Savenije*'s [2011] model. Apparently the differences introduced by using different friction formulations can be compensated by decreasing or increasing the friction coefficient. Therefore, the different analytical models have also been compared with a 1D numerical model in the Scheldt estuary. The calibrated Manning-Strickler friction coefficient K used in the numerical model ($38\ \mathrm{m}^{1/3}\ \mathrm{s}^{-1}$) appears to be almost the same as the friction coefficient of the new model ($39\ \mathrm{m}^{1/3}\ \mathrm{s}^{-1}$), which is to be expected since the new damping equation (27) was obtained by calibration of K against numerical solutions. In Figure 11, all models use the same friction coefficient $K = 38\ \mathrm{m}^{1/3}\ \mathrm{s}^{-1}$. It can be clearly seen that the quasi-nonlinear model [*Savenije et al.*, 2008] and Dronkers' method underestimate the tidal damping while the linear model [*Toffolon and Savenije*, 2011] overestimates it. The reason for the

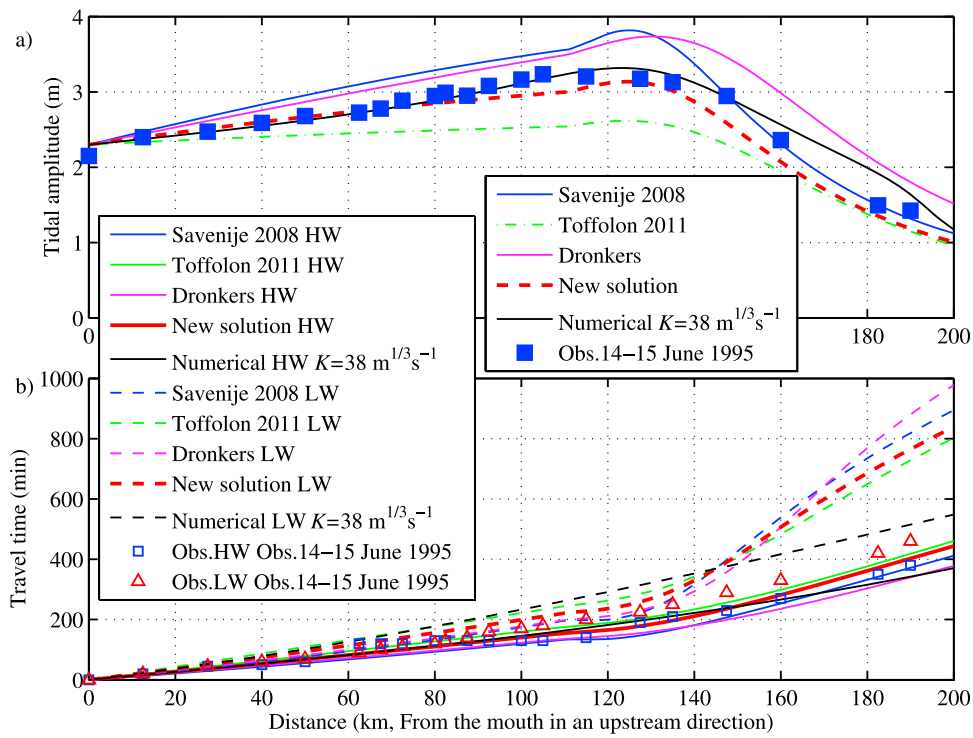

Figure 11. Comparison between different analytical models, numerical solution and field data: (a) tidal amplitude, and (b) travel time at HW and LW in the Scheldt estuary observed on 14–15 June 1995.

overestimation of the travel time at LW in the landward part in both the analytical and numerical models is due to the neglect of river discharge and the high tidal amplitude to depth ratio.

[34] Finally, the tidal characteristics of the Scheldt estuary, as computed with the new model, are presented in diagrams for the velocity number, damping number, celerity number and phase lag. In Figure 12, the Scheldt estuary is represented by red line segments. Next to the segments, the distance from the estuary mouth in kilometers is written, indicating the length over which a segment is representative. We can see that in the Scheldt the seaward part (0–110 km) has a vertical line segment with a constant estuary shape number (this is due to the constant convergence length and depth assumed over that reach). At the inflection point, at 110 km, the tidal wave comes near to a standing wave, but unlike in the method of *Savenije et al.* [2008], this does not happen in the new method. Further upstream the pattern becomes irregular due to shallowing.

5. Results

5.1. Classification of Estuary

[35] Estuaries can be classified on the basis of their water balance, geomorphology, vertical structure of salinity, or hydrodynamics [*Valle-Levinson*, 2010]. The interaction between tidal wave propagation and the geomorphology of the estuary is an important factor for characterizing the type of estuary [*Dyer*, 1997]. *Savenije et al.* [2008] suggest that the classification of estuaries can be based on the result of the imbalance between topographic convergence (i.e., the shape number γ) and friction (i.e., the friction number χ). If convergence is stronger than friction, the wave is amplified; if friction is stronger than convergence, the wave is damped; if their impact is equal, the tidal range is constant and the estuary is indicated as "ideal". In the following, we show that the classification of estuaries can be based on the comparison between tidally averaged depth $\overline{h}$ and ideal depth h_{ideal} which is defined as the depth corresponding to an ideal estuary obtained keeping all the other characteristic quantities (say, tidal amplitude at the mouth, convergence length, friction coefficient) fixed. In particular, an estuary can be characterized as amplified when $\overline{h} > h_{ideal}$, while it is a damped estuary for $\overline{h} < h_{ideal}$, and an ideal estuary for $\overline{h} = h_{ideal}$.

[36] The marginal condition for tidal wave amplification is easily set by posing $\delta = 0$ (hence $\lambda = 1$ and $\tan(\varepsilon) = 1/\lambda$). The resulting relationship between the friction number χ and the shape number γ in the current model is:

$$\chi = \frac{\gamma}{\frac{8}{9\pi}\sqrt{\frac{1}{\gamma^2+1}} + \frac{2}{3(\gamma^2+1)}}, \tag{29}$$

where, substituting (6) into (11), the friction number reads:

$$\chi = r_s \frac{g c_0}{K^2 \omega \overline{h}^{4/3}[1-(4\zeta/3)^2]}\zeta. \tag{30}$$

In the case of a small tidal amplitude to depth ratio ζ, equation (30) corresponds to the definition by *Toffolon et al.* [2006] and *Toffolon and Savenije* [2011].

[37] Substitution of equation (29) into equation (30) yields the expressions of the ideal depth h_{ideal} as a function of tidal

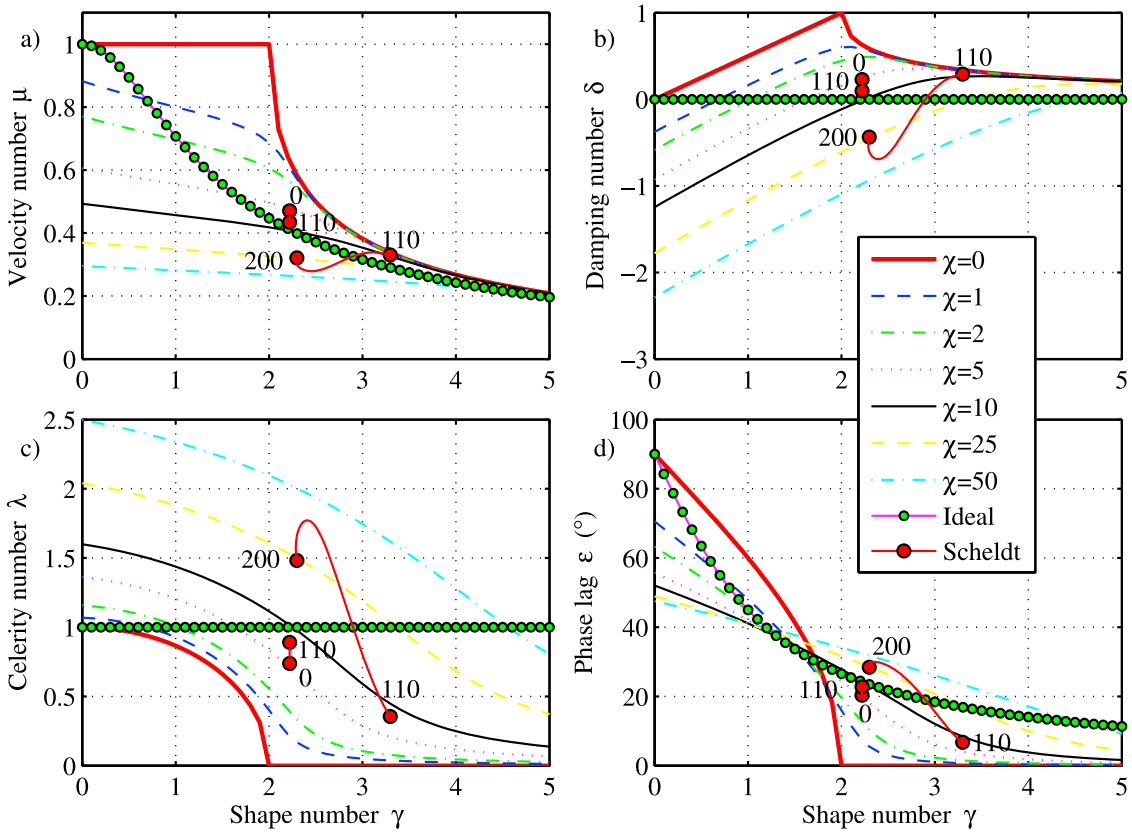

Figure 12. Positioning of the Scheldt estuary (red circles) in: (a) velocity number diagram, (b) damping number diagram, (c) celerity number, and (d) phase lag diagram. The numbers at the inflection points indicate the distance from the estuary mouth (in kilometers). The background shows the lines of the new model with different values of the friction number χ (6). The drawn line with dots represents the ideal estuary.

amplitude η, frequency ω, convergence length a, and friction K:

$$h_{ideal} = f(\eta, \omega, a, K). \tag{31}$$

It is easy to solve equation (31) by a simple numerical algorithm, e.g., Newton's iteration method, since the convergence is usually fast. Figure 13 shows the tidally averaged reference depth $\overline{h}$, the ideal depth h_{ideal} calculated by equation (31), and the critical depth $h_{critical}$ introduced in the next section. The classification of some estuaries in the world, based on the relative quantity $(\overline{h} - h_{ideal})/\overline{h}$ to assess the magnitude of amplification or damping, is presented in Table 2. It can be seen from Figure 13 that most of the estuaries, such as Bristol Channel, Outer Bay of Fundy, Scheldt and St. Lawrence, are significantly amplified estuaries because of the bigger positive relative difference between tidally averaged depth and ideal depth, while Fraser, Ord, Gambia, Pungue, Lalang, Tha Chin, and Chao Phya can be classified as damped estuaries due to negative relative difference. Finally, it is easy to see that Gironde, Hudson, Potomac, Maputo are very close to an ideal estuary. The correspondence of this classification with field observations is consistent, as confirmed by the references indicated in Table 2. The earlier studies of *Toffolon et al.* [2006] and *Savenije et al.* [2008] showed that the estuarine classification can be based on two dimensionless parameters γ and χ. Although results are obviously consistent, the present study yields a dimensional classification system.

5.2. Effect of Depth Variations on Tidal Dynamics in Real Estuaries

[38] The relatively simple analytical solution proposed in this paper is powerful to obtain first-order estimates of the consequences of estuary geometry variations: it is a useful practical tool for management purposes, since it provides a rapid assessment of the tidal behavior of an estuary in response to external or internal modifications.

[39] In particular, intensive dredging along the estuary, which changes the estuary topography, has a measurable impact on the tidal propagation and the damping through the variation of the depth. In addition, it has a direct relation to salt intrusion and storm surge propagation into the estuary. Also sea-level rise can modify the tidally averaged depth $\overline{h}$, thus producing effects that are qualitatively similar to those of dredging. *Church and White* [2006] estimated an increase of global sea-level ranging from 0.28 to 0.34 m from 1990 to 2100 based on the multi-century sea-level records, while projections for UK estuaries exceed 0.5 m at the end of the century for high emissions scenarios considering also vertical land movement [*Lowe et al.*, 2009].

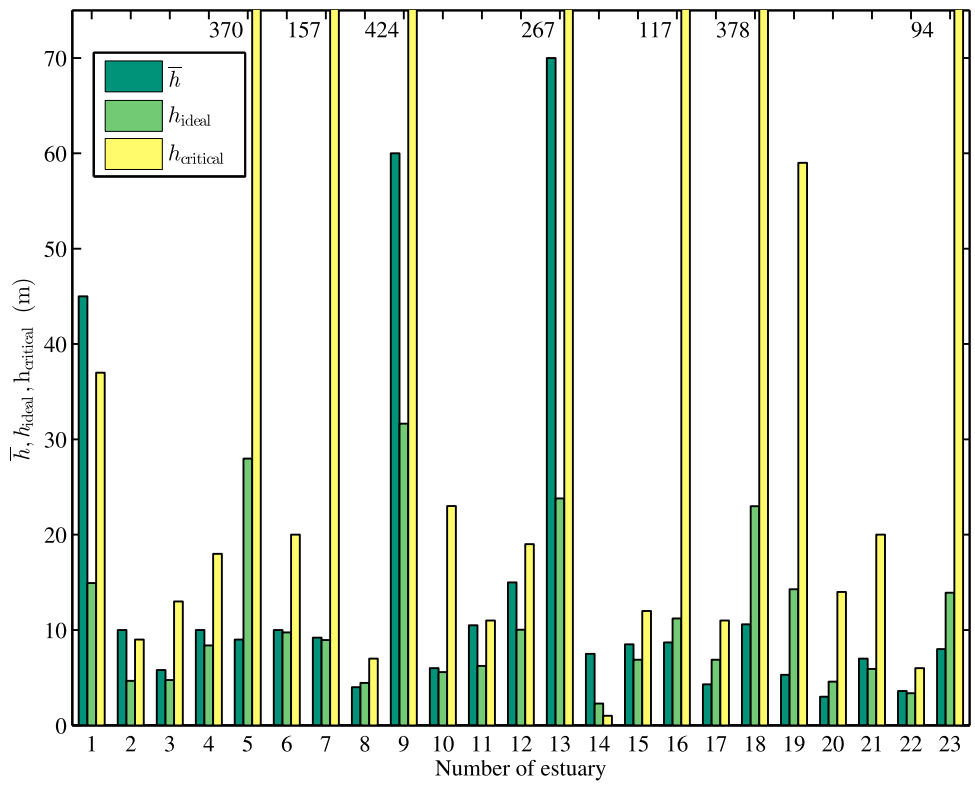

Figure 13. Values of the characteristic depths for the estuaries presented in Table 2: tidally averaged depth $\overline{h}$, ideal depth h_{ideal} from (31), critical depth $h_{critical}$ obtained by the condition (32). Bar for $h_{critical}$ are truncated and higher values are indicated by numbers. The physical meaning is as follows: if $\overline{h} > h_{ideal}$ the estuary is amplified ($\overline{h} < h_{ideal}$ implying damping); if $\overline{h} > h_{critical}$ the estuary is over-amplified.

Table 2. Characteristic Values of Alluvial Estuaries and Classification

Estuary Number	Estuary[a]	T (hour)	η_0 (m)	$\overline{h}$ (m)	a (km)	K ($m^{1/3}$ s^{-1})	ζ	γ	χ	h_{ideal} (m)	$(\overline{h} - h_{ideal})/\overline{h}$	$h_{critical}$ (m)	Type	Ref.[b]
1	Bristol Channel	12.4	2.6	45	65	33	0.06	2.30	0.48	14.9	0.67	37	Over-amplified	1
2	Columbia	12.4	1	10	25	38	0.10	2.81	2.21	4.7	0.53	9	Over-amplified	2
3	Delaware	12.5	0.64	5.8	40	51	0.11	1.35	2.21	4.8	0.18	13	Amplified	3
4	Elbe	12.4	2	10	42	43	0.20	1.68	3.79	8.4	0.16	18	Amplified	4
5	Fraser	12.4	1.5	9	215	31	0.17	0.31	6.28	28.0	−2.11	370	Damped	1
6	Gironde	12.4	2.3	10	44	38	0.23	1.60	5.52	9.8	0.02	20	Close to ideal	5
7	Hudson	12.4	0.69	9.2	140	67	0.08	0.48	0.58	8.9	0.03	157	Close to ideal	1
8	Ord	12	2.5	4	15.2	50	0.63	2.83	54.5	4.5	−0.11	7	Damped	6
9	Outer Bay of Fundy	12.4	2.1	60	230	33	0.04	0.75	0.23	31.7	0.47	424	Amplified	1
10	Potomac	12.4	0.65	6	54	56	0.11	1.01	1.75	5.6	0.07	23	Close to ideal	1
11	Scheldt	12.4	1.9	10.5	27	39	0.18	2.67	3.35	6.2	0.41	11	Amplified	7
12	Severn	12.4	3	15	41	40	0.20	2.10	3.09	10.0	0.33	19	Amplified	8
13	St. Lawrence	12.4	2.5	70	183	44	0.04	1.02	0.11	23.8	0.66	267	Amplified	1
14	Tees	12	1.5	7.5	5.5	36	0.20	10.7	6.62	2.3	0.69	1	Over-amplified	9
15	Thames	12.3	2	8.5	25	31	0.24	2.57	9.94	6.9	0.19	12	Amplified	7
16	Gambia	12.4	0.6	8.7	121	42	0.07	0.54	1.43	11.2	−0.29	117	Damped	7
17	Pungue	12.4	3	4.3	20	31	0.70	2.31	341	6.9	−0.60	11	Damped	7
18	Lalang	12.4	1.5	10.6	217	40	0.14	0.33	2.73	23.0	−1.17	378	Damped	7
19	Tha Chin	12.4	1.35	5.3	87	34	0.25	0.59	13.47	14.3	−1.69	59	Damped	7
20	Incomati	12.4	0.5	3	42	50	0.17	0.92	6.14	4.6	−0.53	14	Damped	7
21	Limpopo	12.4	0.55	7	50	43	0.08	1.18	1.82	5.9	0.15	20	Amplified	7
22	Maputo	12.4	1.4	3.6	16	48	0.39	2.64	17.0	3.4	0.06	6	Close to ideal	7
23	Chao Phya	12.4	0.9	8	109	35	0.11	0.58	3.55	13.9	−0.74	94	Damped	7

[a]Data are modified from *Toffolon et al.* [2006], where data in columns L_b and C_h were listed in a wrong way due to editing mistakes.
[b]Reference where the classification is confirmed: 1, *Prandle* [1985]; 2, *Giese and Jay* [1989]; 3, *Friedrichs and Aubrey* [1994]; 4, *Savenije et al.* [2008]; 5, *Allen et al.* [1980]; 6, *Wright et al.* [1973]; 7, *Savenije* [1992b]; 8, *Uncles* [1981]; 9, *Lewis and Lewis* [1987].

Table 3. Variation of Tidal Amplitude $\Delta\eta$, Velocity Amplitude $\Delta\upsilon$, Wave Celerity Δc, and Phase Lag $\Delta\epsilon$ at Two Locations After an Increase of the Average Depth of 3 m

Estuary Number	Estuary	$\Delta\eta$ (m)		$\Delta\upsilon$ (m/s)		Δc (m/s)		$\Delta\epsilon$ (°)	
		$x = 0$	$x = 50$ km	$x = 0$	$x = 50$ km	$x = 0$	$x = 50$ km	$x = 0$	$x = 50$ km
1	Bristol Channel	0	−0.05	−0.06	−0.09	105.49	91.87	−0.83	−1.06
2	Columbia	0	−0.09	−0.11	−0.17	110.36	92.33	−2.40	−3.46
3	Deltaware	0	0.18	−0.05	0.06	3.27	2.69	−7.90	−7.70
4	Elbe	0	0.33	−0.05	0.07	4.36	3.29	−7.21	−6.39
5	Fraser	0	0.19	0	0.09	0.84	0.48	2.23	1.45
6	Gironde	0	0.40	−0.04	0.11	3.06	2.30	−5.80	−5.22
7	Hudson	0	0.05	−0.06	−0.02	0.25	0.24	1.72	1.26
8	Ord	0	1.29	−0.12	0.13	24.10	11.62	−24.27	−15.11
9	Outer Bay of Fundy	0	0.01	−0.02	−0.02	0.13	0.13	−0.17	−0.16
10	Potomac	0	0.15	−0.05	0.06	1.38	1.21	−2.42	−3.24
11	Scheldt	0	−0.07	−0.19	−0.24	52.22	40.48	−5.77	−7.55
12	Severn	0	0.19	−0.12	−0.05	14.23	9.54	−8.28	−7.40
13	St. Lawrence	0	0	−0.02	−0.02	0.24	0.24	−0.53	−0.51
14	Tees	0	−0.04	−0.05	−0.05	878.26	841.05	−0.06	−0.07
15	Thames	0	0.31	−0.14	−0.04	17.64	11.65	−11.85	−10.78
16	Gambia	0	0.07	−0.03	0.02	0.55	0.44	2.22	1.25
17	Pungue	0	1.55	0.37	0.38	3.94	1.40	−17.2	−8.35
18	Lalang	0	0.15	−0.02	0.06	0.65	0.42	2.78	1.90
19	Tha Chin	0	0.34	0.02	0.17	1.20	0.59	0.40	−0.68
20	Incomati	0	0.27	−0.03	0.16	1.88	1.23	−4.08	−5.68
21	Limpopo	0	0.11	−0.03	0.04	1.84	1.61	−4.00	−4.39
22	Maputo	0	0.50	−0.27	−0.09	36.4	23.7	−19.6	−17.8
23	Chao Phya	0	0.14	−0.02	0.06	0.88	0.59	1.55	0.56

[40] To demonstrate the potential of the analytical method to evaluate the effect of deepening, we applied a depth increase of 3 m to the estuaries listed in Table 2. For simplicity, we assume that the tidal amplitude at the estuary mouth is unchanged by deepening. It is worth noting that *Garrett and Greenberg* [1977] showed how a change of tidal amplitude at the open boundary may be estimated and used to correct predictions of changes in tidal dynamics that might be brought about by the structures, such as tidal power development. Table 3 shows the effect of this deepening on tidal amplitude η, velocity amplitude υ, wave celerity c, and phase lag ϵ at two fixed positions in the estuaries ($x = 0$ and $x = 50$ km). We can see that the response of these quantities to an increase of the depth is quite variable from case to case, while the wave celerity is always increased with larger depth. It is attractive to assess the influence of increasing depth on tidal variables through the diagrams of the velocity number μ, the damping number δ, the celerity number λ, and the phase lag ϵ (see Figures 7–10) as a function of γ and χ. Since the shape number γ is increased with depth, what we need to do is to determine the influence of depth on the friction number χ according to equation (30). At the mouth of estuary ($x = 0$), it is easy to estimate the influence of dredging on tidal variables keeping the tidal amplitude constant: the friction number χ is decreased and the shape number γ increases due to larger depths.

[41] The effect of deepening on tidal dynamics is not linear: in same cases deepening leads to amplification while in others it leads to a reduction of the tidal amplitudes. Figure 14 shows the variation of the velocity amplitude as a result of deepening by 3 m (a) and a more modest increase of 0.3 m (b) for the same locations $x = 0$ and $x = 50$ km. In Figure 14a, corresponding to a depth increase of 3 m, it can be seen that the velocity at the estuary mouth is generally decreased as a result of dredging except in the Fraser, Pungue, and Tha Chin, while the velocity at $x = 50$ km increases with depth for most of the estuaries. Whether the velocity is increased or not depends on the position of the new values of γ andχ in the graph for the velocity number (Figure 7). The extremely high celerity in the Tees (see Table 3, No. 14) is attributed to the strong convergence of the estuary ($\gamma = 10.72$), where a standing wave develops and the celerity tends to infinite. A similar behavior can be noticed in Figure 14b for the smaller depth increase (0.3 m), although some exceptions indicate that the behavior is not monotonic and that the trend of velocity amplification or reduction can change during the deepening process (for instance, in the Ord, Severn, Thames and Maputo, indicated by No. 8, 12, 15 and 22, respectively).

[42] Another interesting result we see in Table 3 (deepening of 3 m) is that the tidal amplitude (at $x = 50$ km) increases in most of the estuaries, but that the strongly amplified estuaries experience a reduction of the amplitude: e.g., Bristol Channel, Columbia, Scheldt and Tees. This is unusual since it is generally accepted that the tidal wave is further amplified as a result of the reduced friction induced by larger depth [e.g., *Luo et al.*, 2007; *Cai et al.*, 2012]. To illustrate this phenomenon, we present the trajectory of the damping number δ with increasing depth in Figure 15. It can be seen that the damping numbers of Bristol Channel, Columbia, Scheldt and Tees (No. 1, 2, 11 and 14; note that the position of Scheldt is different from that in Figure 12, where spring tide conditions were considered instead of mean tide) are actually decreasing with larger depth. We see that a depth increase only leads to increased amplification (larger δ) until a maximum value is reached at a critical depth $h_{critical}$ defined by the condition:

$$\frac{\partial\delta}{\partial\bar{h}} = 0. \tag{32}$$

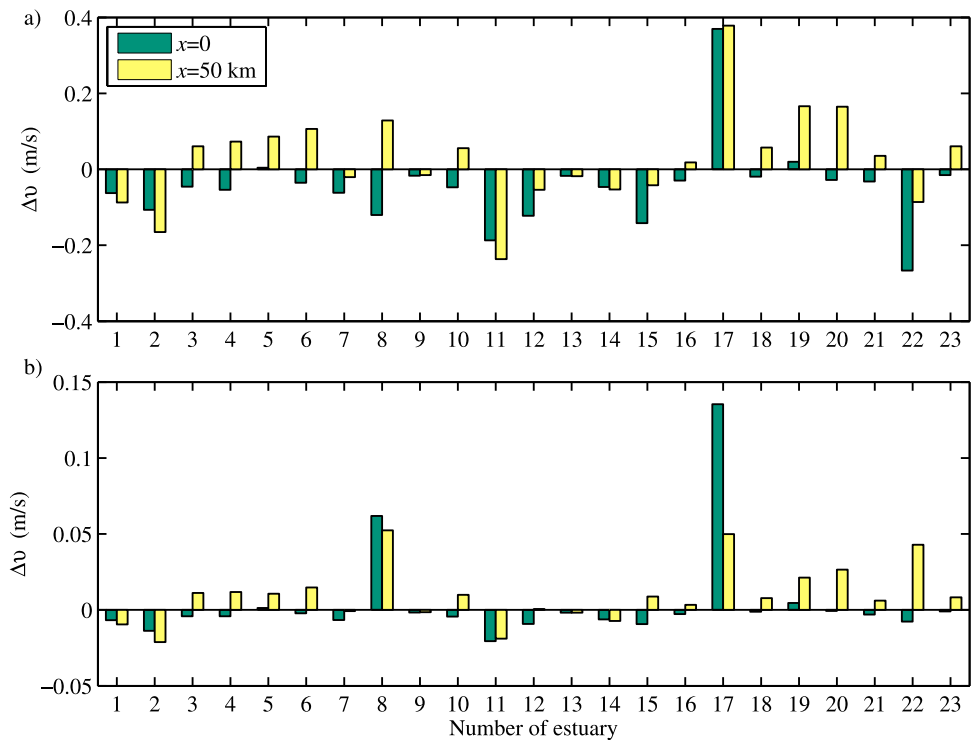

Figure 14. Change of the velocity amplitude at the estuary mouth ($x = 0$) and at $x = 50$ km for: (a) a large increase of the average depth of 3 m, due to dredging; (b) a modest increase of 0.3 m, in agreement with projected sea-level rise for 2100.

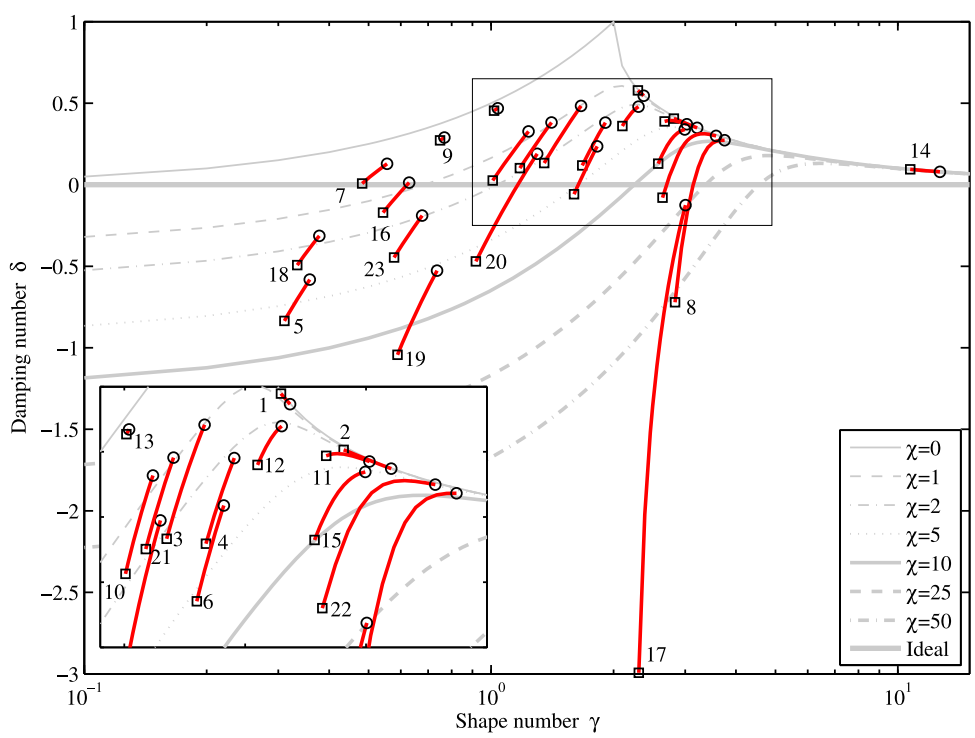

Figure 15. Positioning of the estuaries in Table 2 in the damping number diagram. The black square symbols indicate the initial position before dredging, while the black circle symbols represent the final position after increasing the depth by 3 m. The red segments indicate the trajectories in the (γ, δ) plane. The gray lines indicate the analytical solutions of the new model for different values of the friction number χ (6).

A further increase of the depth leads to a reduction of the amplification until the ideal condition ($\delta = 0$) is reached asymptotically. A similar equation was derived by *Savenije et al.* [2008] for critical convergence (i.e., equation 43 therein), which approximately corresponds to condition (32). The critical convergence was the threshold beyond which the tidal wave acted as a standing wave. We see something similar here. However, unlike the discontinuous behavior predicted by *Savenije et al.* [2008], switching from one wave type to another, the current model provides a continuous solution.

[43] We term estuaries having a depth $\overline{h} > h_{critical}$ as 'over-amplified', a condition typical of strongly convergent (large γ) and relatively weekly dissipative (small χ) estuaries, where increasing the depth reduces the amplification. It is possible to identify this critical depth $h_{critical}$ by changing the depth over a wide range of values in our analytical model until it satisfies condition (32): the calculated values are shown in Table 2. Figure 13 shows the comparison between the tidally averaged depth $\overline{h}$ and the critical depth $h_{critical}$: by comparing the difference between the green and yellow bar, we are able to determine whether an estuary is over-amplified (e.g., Bristol Channel, Columbia, and Tees, indicated by No. 1, 2 and 14, respectively) or not. Generally, with this figure, we are capable of predicting the influence of depth variations on tidal dynamics. This is particularly useful when assessing the influence of human interventions in estuary topography (e.g., dredging) or global sea-level rise on tidal propagation in estuaries, as it influences the aquatic environmental of an estuary and the potential use of water resources.

[44] In Figure 15, we also see that the variation of the damping number in the Bristol Channel, Outer Bay of Fundy, and St. Lawrence (No. 1, 9 and 13, respectively) is very small. This is due to the fact that the tidally averaged depth $\overline{h}$ in these estuaries is very large while the shape number γ, which is increased by dredging, does not change much.

6. Conclusions

[45] In this paper we revisited the analytical approach for tidal hydrodynamics proposed by *Savenije et al.* [2008] by introducing a new tidal damping equation, which is similar to the equation that uses the friction formulation proposed by *Dronkers* [1964]. Reworking this quasi-nonlinear solution, we are able to accurately reproduce the main dynamics of tidal wave propagation along estuary channels. We have also demonstrated that the linear models of *Toffolon and Savenije* [2011] and *Van Rijn* [2011] and the quasi-nonlinear model of *Savenije et al.* [2008] can be readily combined within one consistent theoretical framework, i.e., by solving the same set of equations with different formulations for the friction term. Exploring the difference between the quasi-nonlinear model [*Savenije et al.*, 2008] and the modified linear models proposed by *Toffolon and Savenije* [2011] and *Van Rijn* [2011], we found that the main difference lies in the friction term: the linear model exploits a linear damping equation resulting from a linearized friction term [*Lorentz*, 1926], while the quasi-nonlinear model retains the fully nonlinear friction term, with quadratic velocity and varying depth, but assuming a simple harmonic to determine the tidal velocity at HW and LW. An important difference between the quasi-nonlinear friction term and Dronkers' friction term lies in the fact that Dronkers' friction term does not account for tidally varying depth, while the quasi-nonlinear term does. Another difference is that the approach by *Savenije et al.* [2008] implicitly accounts for the density term, while the other methods neglect the density effect. This has no implications because, as was shown by *Savenije* [2005], the density term cancels out in the derivation of the damping and celerity equations. We further note that the effect of river discharge can, in principle, be incorporated in the present model through a modified formulation, as proposed in *Cai et al.* [2012].

[46] We have compared the performance of the different analytical models with a fully nonlinear numerical model. The comparison indicates that *Savenije et al.* [2008] and *Toffolon and Savenije* [2011] models approach the numerical results from opposite sides (under/overestimating friction). A weighted average of the two comes very close to the numerical results, the optimum weight of the linearized friction term being 1/3, and 2/3 of the quasi-nonlinear friction term. We tested the equations in a real case, the Scheldt estuary, which has strong convergence (overall with γ values above 2, which is the region where the methods show the largest difference). Overall, the new method preforms best against field data and numerical results.

[47] The new model proposed in this paper not only overcomes the unrealistically discontinuous behavior predicted by *Savenije et al.* [2008], but also improves on accuracy compared with linear models as by *Toffolon and Savenije* [2011]. This is important when assessing the influence of depth increase on tidal dynamics in real estuaries (e.g., because of human interventions, by dredging, or sea-level rise). For this purpose, we provided two threshold criteria: the ideal depth h_{ideal} (condition for vanishing damping) and the critical depth $h_{critical}$ (condition for maximum amplification). As a result, we could classify estuaries into three types on the basis of the tidally averaged depth $\overline{h}$ compared with h_{ideal}: damped ($\overline{h} < h_{ideal}$), amplified ($\overline{h} > h_{ideal}$), and approximately ideal ($\overline{h} \simeq h_{ideal}$). Moreover, an estuary can be characterized as over-amplified when it has a depth larger than the $h_{critical}$: in this case, a further increase of the depth reduces the tidal wave amplification.

Appendix A: Derivation of the Linear Tidal Damping Equation by the Envelope Method

[48] Using a Lagrangean approach for the analysis of tidal flow instead of the more common Eulerian one, as proposed by *Savenije* [2005], the continuity equation can be written as

$$\frac{dU}{dt} = r_s \frac{c}{h}\frac{dh}{dt} - \frac{cU}{a} + cU\frac{1}{\eta}\frac{d\eta}{dx}. \tag{A1}$$

The momentum equation can be written in a Lagrangean reference frame as well, providing the differential equation

$$\frac{dU}{dt} + g\frac{\partial h}{\partial x} + g(I_b - I_r) + g\frac{U|U|}{K^2 h^{4/3}} = 0. \tag{A2}$$

where I_r is the water level residual slope resulting from the density gradient.

[49] Combination of equations (A1) and (A2), and using $U = dx / dt$ yields:

$$r_s \frac{cU}{gh}\frac{dh}{dx} - \frac{cU}{g}\left(\frac{1}{a} - \frac{1}{\eta}\frac{d\eta}{dx}\right) + \frac{\partial h}{\partial x} + I_b - I_r + \frac{U|U|}{K^2 h^{4/3}} = 0. \quad \text{(A3)}$$

[50] If we consider the situation at HW and LW, then the following relations apply. The tidal range H ($H = 2\eta$) is the difference between h_{HW} and h_{LW}:

$$2\frac{d\eta}{dx} = \frac{dh_{HW}}{dx} - \frac{dh_{LW}}{dx}, \quad \text{(A4)}$$

where $\overline{h}$ is the tidal average water level. Moreover, at HW and LW

$$\left.\frac{\partial h}{\partial t}\right|_{HW,LW} = 0 \quad \text{(A5)}$$

by definition, and hence

$$\frac{dh_{HW,LW}}{dx} = \left.\frac{\partial h}{\partial x}\right|_{HW,LW}. \quad \text{(A6)}$$

[51] If the dimensionless tidal wave (scaled by the tidal range) is considered undeformed (which is the case when $\eta/\overline{h} \ll 1$), the damping is symmetrical with respect to the tidal average water level $\overline{h}$, which may still have a residual slope $I = d\overline{h}/dx$ such that

$$\frac{dh_{HW}}{dx} + \frac{dh_{LW}}{dx} \approx 2\frac{d\overline{h}}{dx} = 2I, \quad \text{(A7)}$$

with

$$h_{HW} \approx \overline{h} + \eta, \quad h_{LW} \approx \overline{h} - \eta \quad \text{(A8)}$$

These three approximations are not critical to the derivation, and acceptable if $\eta/\overline{h} \ll 1$.

[52] For the tidal velocity at HW and LW the expressions (25) can be derived. Furthermore, we have to realize that the celerities of propagation at HW (c_{HW}) and LW (c_{LW}) are not equal (as a result of the different depths), but we may also assume that they are symmetrical compared to the tidal average wave celerity c, and hence that for small tidal amplitudes

$$\frac{c_{HW}}{h_{HW}} \approx \frac{c_{LW}}{h_{LW}} \approx \frac{c}{\overline{h}}, \quad \text{(A9)}$$

$$c_{HW} + c_{LW} \approx 2c. \quad \text{(A10)}$$

[53] In order to compare the solution obtained using *Savenije* [2005] approach with the linear models, we adopt the usual Lorentz's linearization of the bed shear stress [*Lorentz*, 1926],

$$\frac{U|U|}{K^2 h^{4/3}} = \frac{8}{3\pi}\frac{v}{K^2 \overline{h}^{4/3}} U. \quad \text{(A11)}$$

Combination of equations (A3), (A6), and (25) yields the following expression for the envelope curve at HW:

$$\frac{r_s c_{HW} v \sin(\epsilon)}{g(\overline{h}+\eta)}\frac{dh_{HW}}{dx} - \frac{c_{HW} v \sin(\epsilon)}{g}\left(\frac{1}{a} - \frac{1}{\eta}\frac{d\eta}{dx}\right) + \\ + \frac{dh_{HW}}{dx} + \frac{8}{3\pi}\frac{v^2 \sin(\epsilon)}{K^2 \overline{h}^{4/3}} = -I_b + I_r. \quad \text{(A12)}$$

Similarly, combination of equations (A3), (A6), and (25) provides the envelope curve at LW:

$$\frac{-r_s c_{LW} v \sin(\epsilon)}{g(\overline{h}-\eta)}\frac{dh_{LW}}{dx} + \frac{c_{LW} v \sin(\epsilon)}{g}\left(\frac{1}{a} - \frac{1}{\eta}\frac{d\eta}{dx}\right) + \\ + \frac{dh_{LW}}{dx} - \frac{8}{3\pi}\frac{v^2 \sin(\epsilon)}{K^2 \overline{h}^{4/3}} = -I_b + I_r. \quad \text{(A13)}$$

[54] Subtraction of these envelopes, taking into account the assumption of the wave celerity being symmetrical (equations (A9) and (A10)), yields the following expression:

$$\frac{r_s c v \sin(\epsilon)}{\overline{h}}\left(\frac{dh_{HW}}{dx} + \frac{dh_{LW}}{dx}\right) - 2cv\sin(\epsilon)\left(\frac{1}{a} - \frac{1}{\eta}\frac{d\eta}{dx}\right) + \\ + g\frac{d\eta}{dx} + 2f_L\frac{v^2 \sin(\epsilon)}{\overline{h}} = 0, \quad \text{(A14)}$$

where

$$f_L = \frac{8}{3\pi}\frac{g}{K^2 \overline{h}^{1/3}}. \quad \text{(A15)}$$

The parameters between parentheses in the first term of equation (A14) can be replaced by $2I$ of equation (A7), provided $\eta/\overline{h} < 1$. Further elaboration yields

$$\frac{1}{\eta}\frac{d\eta}{dx}\left(\frac{1+\beta}{\beta}\right) = \frac{1}{a} - f_L\frac{v}{\overline{h}c}, \quad \text{(A16)}$$

where $\beta = cv\sin(\epsilon)/(g\eta)$ is a tidal Froude number.

[55] By scaling, the linear damping equation (A16) reads:

$$\delta = \frac{\mu^2}{1+\mu^2}\left(\gamma - \frac{8}{3\pi}\chi\mu\lambda\right). \quad \text{(A17)}$$

Making use of the trigonometric equation $[\cos(\epsilon)]^{-2} = 1 + [\tan(\epsilon)]^2$, the phase lag and scaling equations ((15) and (14) in section 2) can be combined to eliminate the variable ϵ to give

$$(\gamma - \delta)^2 = \frac{1}{\mu^2} - \lambda^2. \quad \text{(A18)}$$

Introducing the celerity equation (16) and equation (A17) into equation (A18), we end up with:

$$\lambda\left[\delta\lambda\left(1 - \frac{1}{\mu^2}\right) + \frac{8}{3\pi}\chi\mu\left(1 - \lambda^2\right)\right] = 0, \quad \text{(A19)}$$

which can be simplified for $\lambda \neq 0$. Subsequently, equation (A19) along with equation (A17) yields a simple relationship between δ and μ, λ:

$$\delta = \frac{\gamma}{2} - \frac{4}{3\pi}\frac{\chi\mu}{\lambda}, \tag{A20}$$

which is reported as (18) in section 3.1.

Appendix B: Derivation of the Tidal Damping Equation Using Dronkers' Friction Formulation by the Envelope Method

[56] Higher order formulation, like that proposed by *Dronkers* [1964], can be represented using Chebyshev polynomials as follows:

$$\frac{U|U|}{K^2 h^{4/3}} = \frac{16}{15\pi}\frac{\upsilon^2}{K^2 \overline{h}^{4/3}}\left[\frac{U}{\upsilon} + 2\left(\frac{U}{\upsilon}\right)^3\right]. \tag{B1}$$

Here it has been assumed that the effect of the periodic variation of the depth may be disregarded and that the average depth may be used instead, as long as the tidal amplitude to depth ratio is small. Applying equation (B1) in the derivation of damping equation as described in the Appendix A, one can easily obtain the following expression:

$$\delta = \frac{\mu^2}{1+\mu^2}\left(\gamma - \frac{16}{15\pi}\chi\mu\lambda - \frac{32}{15\pi}\chi\mu^3\lambda^3\right). \tag{B2}$$

After some algebra, it is possible to obtain a simpler relation between δ. μ and λ:

$$\delta = \frac{\gamma}{2} - \frac{8}{15\pi}\frac{\chi\mu}{\lambda} - \frac{16}{15\pi}\chi\mu^3\lambda. \tag{B3}$$

Notation

The following symbols are used in this paper:

- a convergence length of cross-sectional area
- $\overline{A}$ tidally averaged cross-sectional area of flow;
- $\overline{A_0}$ tidally averaged cross-sectional area at the estuary mouth;
- $\overline{B}$ width;
- B_s storage width;
- c wave celerity;
- c_0 celerity of a frictionless wave in a prismatic channel;
- c_{HW} wave celerity at HW;
- c_{LW} wave celerity at LW;
- f friction factor accounting for the difference in friction at HW and LW;
- f_L friction factor used for the derivation of linear damping equation;
- F quadratic friction term;
- F_L Lorentz's friction term;
- F_D Dronker's friction term;
- $\hat{F}_S$ effective friction term obtained with a Lagrangean-based approach;
- g acceleration due to gravity;
- h cross-sectional average depth;
- $\overline{h}$ tidal average depth;
- h_{ideal} ideal depth;
- $h_{critical}$ critical depth;
- h_{HW} depth at HW;
- h_{LW} depth at LW;
- H tidal range;
- I tidally averaged water level slope;
- I_b bottom slope;
- I_r water level residual slope due to the density gradient;
- K Manning-Strickler friction factor;
- L estuary length;
- Q tidal discharge;
- r_s storage width ratio;
- t time;
- T tidal period;
- U cross-sectional average flow velocity;
- U_{HW} tidal velocity at HW;
- U_{LW} tidal velocity at LW;
- x distance;
- x^* dimensionless distance;
- z tidal water level variation;
- α weight of the linearized friction term;
- β tidal Froude number;
- γ estuary shape number;
- δ damping number;
- ϵ phase lag between HW and HWS (or LW and LWS);
- ζ tidal amplitude at the estuary mouth;
- η tidal amplitude;
- η_0 tidal amplitude at the estuary mouth;
- λ celerity number;
- μ velocity number;
- υ tidal velocity amplitude;
- χ friction number;
- ω tidal frequency.

[57] **Acknowledgments.** The authors would like to thank the two anonymous referees for their valuable comments and suggestions, which have greatly improved this paper. The work of the third author has been partially cofunded by the Italian Ministry of Education, University and Research (MIUR) within the project 'Eco-morfodinamica di ambienti a marea e cambiamenti climatici' (PRIN 2008). The first author is financially supported during his PhD program by the China Scholarship Council with the project reference number of 2010638037.

References

Allen, G. P., J. C. Salomon, P. Bassoullet, Y. Dupenhoat, and C. Degrandpre (1980), Effects of tides on mixing and suspended sediment transport in macro-tidal estuaries, *Sediment. Geol.*, *26*(1–3), 69–90.

Cai, H., H. H. G. Savenije, Q. S. Yang, S. Y. Ou, and Y. P. Lei (2012), The influence of river discharge and dredging on tidal wave propagation; The Modaomen estuary case, *J. Hydraul. Eng.*, doi:10.1061/(ASCE)HY.1943-7900.0000594, in press.

Cartwright, D. E. (1968), A unified analysis of tides and surges round north and east Britain, *Philo. Trans. R. Soc. London A*, *263*, 1–55.

Church, J. A., and N. J. White (2006), A 20th century acceleration in global sea-level rise, *Geophys. Res. Lett.*, *33*, L01602, doi:10.1029/2005GL024826.

Dronkers, J. J. (1964), *Tidal Computations in River and Coastal Waters*, pp. 296–304, Elsevier, New York.

Dyer, K. R. (1997), *Estuaries: A Physical Introduction*, 2nd ed., pp. 31–40, John Wiley, New York.

Friedrichs, C. T. (2010), Barotropic tides in channelized estuaries, in *Contemporary Issues in Estuarine Physics*, edited by A. Valle-Levinson, pp. 27–61, Cambridge Univ. Press, Cambridge, UK.

Friedrichs, C. T., and D. G. Aubrey (1994), Tidal propagation in strongly convergent channels, *J. Geophys. Res.*, *99*(C2), 3321–3336.

Garrett, C., and D. Greenberg (1977), Predicting changes in tidal regime: The open boundary problem, *J. Phys. Oceanogr.*, *7*(2), 171–181.

Giese, B. S., and D. A. Jay (1989), Modeling tidal energetics of the Columbia river estuary, *Estuarine Coastal Shelf Sci.*, *29*(6), 549–571.

Horrevoets, A. C., H. H. G. Savenije, J. N. Schuurman, and S. Graas (2004), The influence of river discharge on tidal damping in alluvial estuaries, *J. Hydrol.*, *294*(4), 213–228.

Jay, D. A. (1991), Green law revisited: Tidal long-wave propagation in channels with strong topography, *J. Geophys. Res.*, *96*(C11), 20,585–20,598.

Lanzoni, S., and G. Seminara (1998), On tide propagation in convergent estuaries, *J. Geophys. Res.*, *103*(C13), 30,793–30,812.

Lewis, R. E., and J. O. Lewis (1987), Shear-stress variations in an estuary, *Estuarine Coastal Shelf Sci.*, *25*(6), 621–635.

Lorentz, H. A. (1926), *Verslag Staatscommissie Zuiderzee*, Algemene Landsdrukkerij, The Hague, Netherlands.

Lowe, J. A., et al. (2009), UK Climate Projections science report: Marine and coastal projections, Met Office Hadley Centre, Exeter, UK.

Luo, X. L., E. Y. Zeng, R. Y. Ji, and C. P. Wang (2007), Effects of in-channel sand excavation on the hydrology of the Pearl River Delta, China, *J. Hydrol.*, *343*(3–4), 230–239.

Prandle, D. (1985), Classification of tidal response in estuaries from channel geometry, *Geophys. J. R. Astron. Soc.*, *80*(1), 209–221.

Prandle, D. (2003), Relationships between tidal dynamics and bathymetry in strongly convergent estuaries, *J. Phys. Oceanogr.*, *33*(12), 2738–2750.

Prandle, D. (2009), *Estuaries: Dynamics, Mixing, Sedimentation and Morphology*, 236 pp., Cambridge Univ. Press, New York.

Savenije, H. H. G. (1992a), Lagrangian solution of St Venants equations for alluvial estuary, *J. Hydraul. Eng.*, *118*(8), 1153–1163.

Savenije, H. H. G. (1992b), Rapid assessment technique for salt intrusion in alluvial estuaries, Ph.D. thesis, Int. Inst. for Infrastructure, Hydraul. and Environ., Delft, Netherlands.

Savenije, H. H. G. (1993), Determination of estuary parameters on basis of Lagrangian analysis, *J. Hydraul. Eng.*, *119*(5), 628–642.

Savenije, H. H. G. (1998), Analytical expression for tidal damping in alluvial estuaries, *J. Hydraul. Eng.*, *124*(6), 615–618.

Savenije, H. H. G. (2001), A simple analytical expression to describe tidal damping or amplification, *J. Hydrol.*, *243*(3–4), 205–215.

Savenije, H. H. G. (2005), *Salinity and Tides in Alluvial Estuaries*, pp. 23–107, Elsevier, New York.

Savenije, H. H. G., and E. J. M. Veling (2005), Relation between tidal damping and wave celerity in estuaries, *J. Geophys. Res.*, *110*, C04007, doi:10.1029/2004JC002278.

Savenije, H. H. G., M. Toffolon, J. Haas, and E. J. M. Veling (2008), Analytical description of tidal dynamics in convergent estuaries, *J. Geophys. Res.*, *113*, C10025, doi:10.1029/2007JC004408.

Toffolon, M., and H. H. G. Savenije (2011), Revisiting linearized one-dimensional tidal propagation, *J. Geophys. Res.*, *116*, C07007, doi:10.1029/2010JC006616.

Toffolon, M., G. Vignoli, and M. Tubino (2006), Relevant parameters and finite amplitude effects in estuarine hydrodynamics, *J. Geophys. Res.*, *111*, C10014, doi:10.1029/2005JC003104.

Uncles, R. J. (1981), A note on tidal asymmetry in the Severn estuary, *Estuarine Coastal Shelf Sci.*, *13*(4), 419–432.

Valle-Levinson, A. (2010), Definition and classification of estuaries, in *Contemporary Issues in Estuarine Physics*, edited by A. Valle-Levinson, pp. 1–10, Cambridge Univ. Press, Cambridge, UK.

Van Rijn, L. C. (2011), Analytical and numerical analysis of tides and salinities in estuaries; part I: tidal wave propagation in convergent estuaries, *Ocean Dyn.*, *61*, 1719–1741, doi:10.1007/s10236-011-0453-0.

Vignoli, G., M. Toffolon, and M. Tubino (2003), Non-linear frictional residual effects on tide propagation, in *Proceedings of XXX IAHR Congress*, vol. A, pp. 291–298, Int. Assoc. of Hydraul. Eng. and Res., Madrid, Spain.

Wright, L. D., J. M. Coleman, and B. G. Thom (1973), Processes of channel development in a high-tide-range environment - Cambridge Gulf-Ord River Delta, Western Australia, *J. Geol.*, *81*(1), 15–41.